

**EFFECT OF THE E11 AMINO ACID ON THE LIGAND  
BINDING IN HEMOGLOBIN I FROM *LUCINA PECTINATA***

by

Laura B. Granell-Ortiz

A thesis submitted in partial fulfillment of the requirements for the degree of

MASTER OF SCIENCE

in

CHEMISTRY

UNIVERSITY OF PUERTO RICO

MAYAGÜEZ CAMPUS

2007

Approved by:

\_\_\_\_\_  
Jorge L. Ríos-Steiner, Ph.D.  
Member, Graduate Committee

\_\_\_\_\_  
Date

\_\_\_\_\_  
José E. Cortés-Figueroa, Ph.D.  
Member, Graduate Committee

\_\_\_\_\_  
Date

\_\_\_\_\_  
Juan López-Garriga, Ph.D.  
President, Graduate Committee

\_\_\_\_\_  
Date

\_\_\_\_\_  
Nilda E. Aponte, Ph.D.  
Graduate Student Representative

\_\_\_\_\_  
Date

\_\_\_\_\_  
Francis Patrón, Ph.D.  
Chairperson, Chemistry Department

\_\_\_\_\_  
Date

## ABSTRACT

Hemoglobin I (HbI) from *Lucina pectinata* (clam) is a protein that binds and transports H<sub>2</sub>S to the bacteria in the clam. HbI is one of the few known hemoglobins that carries H<sub>2</sub>S, toxic gas, in its active site, which contains a GlnE7, PheB10, PheCD1 and PheE11. The stabilization of bound ligands, including H<sub>2</sub>S, appears to be dictated by the flexibility of the unusual distal heme pocket environment. Therefore, to define the role of the PheE11 on heme-ligand stability, FT-IR and kinetics studies were performed on HbI PheE11Val, PheE11Gln and PheE11Tyr using CO as ligand. The HbI PheE11Gln exhibited three stretching vibrational frequencies in the FT-IR spectrum: 1960 cm<sup>-1</sup> (22%), 1948 cm<sup>-1</sup> (15%), and 1939 cm<sup>-1</sup> (64%). While, the HbI PheE11Tyr displayed vibrations located at 1962 cm<sup>-1</sup> (34%), 1954 cm<sup>-1</sup> (3%), and 1941 cm<sup>-1</sup> (63%). The HbI PheE11Val showed just two vibrational peaks at 1955 cm<sup>-1</sup> (24%) and 1942 cm<sup>-1</sup> (76%). Each of these frequencies was assigned to different structural conformations. The higher frequencies are assigned as open conformations where no interactions occur. Whereas, lower frequencies were assigned to a closed conformation where the residues at the distal site (B10, E7, and E11) are having direct electrostatic interactions and/or hydrogen bond with the ligand. The results suggest that single site directed mutagenesis of the HbI heme pocket affect synergistically the displacement and orientation of other amino acids in the heme moiety. Also, we suggest that the PheE11 modulate the stabilization of the ligand by steric and hydrophobic interactions between the other nearby residues (GlnE7 and PheB10), and controls ligand migration in HbI.

## RESUMEN

La almeja *Lucina pectinata* contiene varias hemoglobinas entre las cuales se encuentra, Hemoglobina I (HbI), HbI es una proteína monomérica que enlaza y transporta ácido sulfhídrico ( $H_2S$ ). Esta es una de las pocas hemoglobinas que transportan este gas tóxico en su sitio activo. Los residuos en la región distal del grupo hemo: GlnE7, PheB10, PheCD1 y PheE11, parecen ser los responsables de la estabilización del ligando. Se ha demostrado que la matriz proteica muestra cierto grado de flexibilidad lo que permite la estabilización del ligando. Muchos estudios se han realizado para determinar la importancia y función de los amino ácidos en la posición B10 y E7, pero poco se sabe sobre la posición E11. Para definir el papel que desempeña este amino ácido, se llevaron a cabo estudios de infrarrojo y cinéticos utilizando mutantes de HbI, donde la PheE11 fue sustituida por Val, Gln y Tyr. El espectro de IR para HbI PheE11Gln mostró tres bandas vibracionales a:  $1960\text{ cm}^{-1}$  (22%),  $1948\text{ cm}^{-1}$  (15%) y  $1939\text{ cm}^{-1}$  (64%). Mientras que en el mutante HbI PheE11Tyr se observaron vibraciones localizadas en  $1962\text{ cm}^{-1}$  (34%),  $1954\text{ cm}^{-1}$  (3%) y  $1941\text{ cm}^{-1}$  (63%). Sin embargo, el mutante HbI PheE11Val solo presentó dos bandas vibracionales a  $1942\text{ cm}^{-1}$  (76%) y  $1955\text{ cm}^{-1}$  (24%). A cada una de las frecuencias observadas se le ha asignado una conformación diferente del centro activo. Frecuencias altas fueron asignadas a una conformación abierta, donde no hay interacción con el ligando. Mientras que frecuencias bajas fueron atribuidas a una conformación cerrada, donde los residuos en la posición E7 y B10 están teniendo interacciones electrostáticas y/o puentes de hidrógeno con el ligando. Estos resultados sugieren que las mutaciones en el centro activo de HbI afecta sinérgicamente el desplazamiento y orientación de los amino ácidos cercanos al centro activo, que la PheE11 modula la estabilización del ligando mediante interacciones estéricas e hidrofóbicas entre los amino ácidos cercanos al hemo (GlnE7 y PheB10) y controla la migración del ligando.

© 2007 Laura B. Granell-Ortiz

*To my aunt, Silvia Ortiz, and father, Alberto Granell  
for all these years of care, trust, support, friendship, and love.  
To my mother, Pura, for being my inspiration and motivation.*

## ACKNOWLEDGEMENTS

I would like to thank several persons and institutions that collaborated with my research, without their support and advice it would be impossible for me to finish this. First, I would like to thank my advisor, Dr. Juan López-Garriga, for the opportunity of doing research under his supervision, his support, and guidance through this beautiful and interesting scientific world. Second, I would like to thank my committee: Dr. José E. Cortés-Figueroa and Dr. Jorge L. Ríos-Steiner whom gave me time and were available to help me during this path. Third, I would like to thank Ruth Pietri and Cacimar Ramos for my training, experimental assistance, the example, motivation, inspiration, support, and friendship I received for these five years. From these persons, I am completely grateful. I would also like to thanks Joann Vega, Yadira Santiago, Danny Santiago, Debora Acevedo, Elvin Igartúa, Elddie M. Román, María Rodriguez, and Samirah Mercado.

Bridge to Doctorate Program - Alliance to Minory Program (BDP-AMP) and Graduate and Undergraduate Students Enhancing Science and Technology in K-12 Schools (GUEST K-12) are acknowledged for the financial support. At last, but the most important I would like to thank my aunt Silvia Ortiz, my dad, Alberto Granell, my three brothers: Titin, Toño and Kiki, and all my family for their unconditional support, and love.

# Table of Contents

Abstract	ii
Resumen	iii
Acknowledgements	v
Table List	viii
Figure List	ix
1 INTRODUCTION	1
1.1 Hemoglobins: general information	1
1.2 Spectroscopic characteristics of hemoglobins	5
1.3 CO as a probe of heme distal environment	8
1.4 Hemoglobins from <i>Lucina pectinata</i>	15
1.5 Finality of the research	20
2 MATERIALS AND METHODS	21
2.1 Cloning of the HbI mutants	21
2.2 Large-scale expression or fermentation of the HbI mutants	21
2.3 Bacterial lysis and heme protein isolation	25
2.4 Purification of the HbI mutants	26
2.4.1 Affinity Chromatography	26
2.4.2 Size Exclusion Chromatography	29
2.5 Purity of the HbI mutants by SDS-PAGE	31
2.6 Concentration- UV-Vis of the HbI mutants	32
2.7 Fourier Transformed Infrared (FT-IR) studies of HbI mutants	35
2.7.1 Deoxy and carbon monoxide heme complexes preparations	35
2.7.2 FT-IR Measurements	36
2.8 Kinetics studies of HbI mutants	37
2.8.1 Sample preparation and kinetics measurements	37

3 RESULTS	39
3.1 UV-Vis measurements of CO HbI mutants derivatives	39
3.2 FT-IR measurements of CO derivatives	39
3.2.1 FT-IR measurements of CO derivatives with HbI mutants at The position E11	39
3.3 Kinetics rate constant for the dissociation of CO	47
4 DISCUSSION	53
4.1 Interpretation of the CO vibrational frequencies in HbI mutants at the E11 position	53
4.2 Implications of the FT-IR results in ligand-binding and stabilization	58
4.3 Implication and functionality of the PheE11 in HbI	60
5 CONCLUSIONS AND FUTURE WORKS	65
5.1 Conclusions	65
5.2 Future Works	66
REFERENCES	67
APPENDIX A: KINETIC DATA ANALYSIS	70

## Table List

<b>Tables</b>	<b>Page</b>
2.1 The spectral properties: $\lambda_{\max}$ and the corresponding absorptivity coefficients for HbI ferrous and ferric complexes	35
3.1 The CO dissociation observed constants for the rHbI and the HbI mutants at the E11 position	48
4.1 CO stretching frequencies for rHbI, HbI mutants at the E11 position, and SW-Mb	54
4.2 Kinetic dissociation and association constants of CO and O <sub>2</sub> for rHbI and the HbI mutants at the E11 position	59

## Figure List

Figures	Page
1.1 Hemoglobins helical arrangement. (a) three-over-three helical sandwich from horse heart myoglobin (PDB:1DWR). (b) two-over-two helical sandwich from the protozoan <i>Paramecium caudatum</i> , trHbP (PDB:1DLW)	3
1.2 Structure of the heme group, which consist of a porphyrin ring bound to an iron atom (red) in the center. This Fe has six coordination sites, where four are occupied by the nitrogen atoms (blue) of the porphyrin ring and the other two can be occupy by the ligand and histidine at the F8 position.	4
1.3 Structure of the heme pocket from horse heart myoglobin (PDB:1DWR). The area designated (a) and (b) correspond to the distal and the proximal site in the heme pocket, respectively. The heme group (gray) occupies the middle of the pocket. Residues in each of the sites are represented in different colors: ValE11 (yellow), HisE7 (blue), LeuB10, PheCD1 (purple) and His93 (turquoise). The ligand that can occupy the sixth coordination position is indicated by the black arrow. The drawings were made with VDM 1.8.5.	6
1.4 UV-Vis spectra for heme protein, Hemoglobin II (HbII) from <i>Lucina pectinata</i> , which shows the characteristics Soret and Q's bands.	7
1.5 Diagram describing the phenomenon of back-bonding which consist of two parts: (A) in which the carbon of the carbonyl donated two electrons to the vacant Fe d-orbital (Fe designated as M in the diagram), and (B) where the Fe compensate the increased in electron density of the CO electron donation, by interaction of the filled Fe $dz^2$ orbital with the empty $p\pi^*$ orbital on the CO ligand.	10
1.6 Conformational states of mammalian myoglobin where the (- - -) between the HisE7 and the O represents hydrogen bonds. (a) $A_0$ : open conformation with a $\nu_{CO}$ at $1966\text{ cm}^{-1}$ . (b) $A_{1,2}$ : close conformation with a $\nu_{CO}$ at $1945\text{-}1954\text{ cm}^{-1}$ . (c) $A_3$ : close conformation with a $\nu_{CO}$ at $1932\text{ cm}^{-1}$ .	11
1.7 Representation of the resonance structures adopted when the CO is bound to Fe. (a) When there is a positive electric field around the oxygen; presence of back-bonding. (b) When there is a negative electric field around the oxygen; absence of back-bonding. Diagram modified from reference.	13

- 1.8 Inverse correlation diagram of the Fe–CO stretching frequency and the C–O stretching frequency for a variety of heme proteins and porphyrin derivatives. Line (2) are for complexes in which the proximal ligand is a histidine. The shaded figures are for the wild type protein: horseradish peroxidase (●), cytochrome c peroxidase (▨) and myoglobin (▲). The corresponding open figures are obtained from their mutant proteins. 14
- 1.9 Distal heme pocket of metaquo HbI from *Lucina pectinata* (PDB: FLP). The residues at the distal position are identified by a three letter abbreviation and their corresponding position. The drawings were made with VDM 1.8.5. 17
- 1.10 The structures of (a) ferric HbI and (b) HbI-H<sub>2</sub>S complexes. The view from the top of the heme showed the displacement of the distal heme residues (Gln E7 and PheB10). The drawings were made with VDM 1.8.5. 18
- 2.1 Logarithmic bacterial growth curve of the HbI PheE11Val expressed with *E. coli* competent cells. Each point represents an absorption measured at a 30 minutes interval. This curve followed a sigmoidal profile curve fit represented as hatched lines (----) and was calculated by Origin<sup>®</sup> 7.5 software. 24
- 2.2 Elution profile of the metal affinity chromatography used to separate PheE11Val HbI mutant from impurities. The first peak at ~ 100 mL was assigned as impurities. The second major peak was assigned as a mixture of salts (imidazole) and our protein. 28
- 2.3 The Size Exclusion Chromatogram of HbI PheE11Val. The protein elution profile using the UV lamp at 280 nm is represented by (—), and the % conductivity elution profile of the effluent is shown (- - -) The “bump” observed in the (—) is due to the presence of imidazole during the process. 30
- 2.4 SDS- PAGE for some of the HbI mutant at the E11 position. (1) SDS-Page Standard (2) rHbI after SEC (3) HbI PheE11Tyr after SEC (4) PheE11Val HbI mutant after SEC (5) HbI PheE11Val after all the procedure of purification (6) HbI PheE11Tyr after BD Talon<sup>™</sup> (7) PheE11Tyr HbI mutant after desalting (8) HbI PheE11Val after desalting using FPLC (9) HbI PheE11Val after BD Talon<sup>™</sup> (10) HbI PheE11Gln after BD Talon<sup>™</sup>. 33
- 2.5 UV-Vis spectra for the carbon monoxide (—), Deoxy (---) and Metaquo (....) HbI, together with their distinctive Soret and Q bands. 34

- 3.1 UV-Spectra of the HbI mutants at the E11 position with CO as ligand. This spectra shows the Soret band at 421 nm and the Q bands at 539 and 570 nm. 40
- 3.2 The FT-IR spectrum of the CO stretching bands obtained for rHbI. In the spectrum, it is shown the experimental data (red), the best data fit (navy blue), and the residual (pink). The obtained deconvoluted CO stretching bands are shown here: in orange for the A<sub>0</sub> conformer (1960 cm<sup>-1</sup>), light blue for the A<sub>1,2</sub> conformer (1950 cm<sup>-1</sup>), and the one green line for A<sub>3</sub> (1936 cm<sup>-1</sup>). 43
- 3.3 The FT-IR spectrum of the CO stretching bands obtained for the HbI PheE11Val HbI mutant. The spectrum, it is shown the experimental data (red), the best data fit (navy blue), the residual (pink), and the obtained deconvoluted CO stretching bands (green and light blue). 44
- 3.4 The FT-IR spectrum of the CO stretching bands obtained for the PheE11Tyr HbI mutant. In the spectrum, it is shown the experimental data (red), the best data fit (navy blue), the residual (pink), and the obtained deconvoluted CO stretching bands (green and light blue). 45
- 3.5 The FT-IR spectrum of the CO stretching bands obtained for the HbI PheE11Gln HbI mutant. In the spectrum, it is shown the experimental data (red), the best data fit (navy blue), the residual (pink), and the obtained deconvoluted CO stretching bands (green and light blue). 46
- 3.6 Plot of absorbance at 420 nm vs. time for the replacement reaction of CO in rHbI, under flooding conditions where [NO] >> [HbI-CO]. The continuous red shows the best behavior of the experimental data which is described by  $y = 0.6264 e^{-0.008x} - 0.7056$ . 49
- 3.7 Plot of absorbance at 420 nm vs. time for the replacement reaction of CO in HbI PheE11Val, under flooding conditions where [NO] >> [HbI-CO]. The continuous red shows the best behavior of the experimental data which is described by  $y = 1.0060 e^{-0.010x} - 0.4044$ . 50
- 3.8 Plot of absorbance at 420 nm vs. time for the replacement reaction of CO in HbI PheE11Gln, under flooding conditions where [NO] >> [HbI-CO]. The continuous red shows the best behavior of the experimental data which is described by  $y = 0.4038 e^{-0.005x} - 0.1428$ . 51
- 3.9 Plot of absorbance at 420 nm vs. time for the replacement reaction of CO

- in HbI PheE11Tyr, under flooding conditions where  $[\text{NO}] \gg [\text{HbI-CO}]$ . The continuous red shows the best behavior of the experimental data which is described by,  $y = 0.3179 e^{-0.009x} - 0.5919$ . 52
- 4.1 Molecular dynamic scheme of the HbI structure of the (a) wt-HbI, and (b) HbI PheE11Val. The heme group and the residues are show in ball-sticks representations, while the different helices are shown as ribbons. The residue in yellow color is Phe in (a) and Val in (b). 56
- 4.2 Structure of the met-aquo wt-HbI distal pocket (PDB:FLP). The heme group and the residues are displayed as sticks representation. The Phe in the CD1, B10 and E11 position are labeled with the specific position. The dotted lines represent the distances between each amino acid. The drawings were made with VDM 1.8.5. 61
- 4.3 Squematic illustration of the interactions in wt-HbI, where the Phe at the E11, B10 and CD1 are showed in yellow, red and purple, respectively. The Gln at the E7 position is showed in blue, and the arrow represents the CO bound to the Fe. The dotted magenta lines represent the possible steric and hydrophobic interactions of the PheE11 with the GlnE7 and PheB10. The dash gray lines represent the electrostatic interactions of the Phe B10 and CD1 once the PheE11 positionated them in the right way. While the solid black line represent the possible hydrogen bond of the GlnE7 with the CO. 64

# 1 INTRODUCTION

## 1.1 Hemoglobins: general information

For more than one hundred years the scientific community had spent time to understand the structure, function and ligand-binding of hemoglobins (Hbs). This is because this complex molecule can bind oxygen ( $O_2$ ) as well as nitric oxide (NO), carbon monoxide (CO), cyanide ( $CN^-$ ), and hydrogen sulfide ( $H_2S$ ). All these gases have different characteristic, and cause different effects in the organism and physiological functions. For example,  $O_2$  is vital for all living organism in their respiratory processes, while the other gases, NO, CO,  $CN^-$  and  $H_2S$ , are considered highly toxic for many organisms. Thus, it would be very significant and interesting to understand how these heme-proteins bind different kind of molecules without inhibiting their physiological functions.

Hemoglobins have been identified in all kingdoms; vertebrates, invertebrates, prokaryotes (bacterias), eukaryotes and plants. Its functions and mechanisms of ligand-binding differ one from another (1). For example, the most common function of Hbs is to transport and storage  $O_2$  (myoglobin, Mb). However, there are several other Hbs which use NO to control levels of  $O_2$  (nematodes); scavenge  $O_2$  in plants (leghemoglobins); perform NO detoxification by dioxygenation reaction (flavoheemoglobins); sense of  $O_2$  in bacterias; detoxificate from chlorinated materials (from marine worms); bind and transport sulfide complexes to protect itself from toxicity (from mollusk); implicate in signal transduction and gene regulation (cytoglobin and neuroglobins), among others (1,2). The functions of these Hbs are dictated by the size, location in the organism, and residues composition of the entire protein. In general, it has been found that the amino acid composition in monomeric Hbs

vary from 109 to 154 (1). Even though, most of the Hbs exhibit a similar tertiary structure that consist of 6-8  $\alpha$ -helices connected by short loops that form a three-over-three helical sandwich (3), it has been found that truncated hemoglobins (trHbs), Hbs from microorganism, contain a two-over-two helical sandwich motif (2). Figure 1.1 shows the two helical arrangements, where (a) cooresponded to the three-over-three helical sandwich from horse heart myoglobin, and (b) to the two-over-two helical sandwich from *Paramecium caudatum* (trHbP). The heme group in all these Hbs is bound to the structure. Along with all these variations, there are two completely conserved amino acids in these heme-proteins: a phenylalanine (Phe) residue at position CD1 and a histidine (His) at position F8. Residues along all the protein play a role in protein stabilization, ligand-binding, structure folding, and physiological functions. For example, apolar residues at CD1, E11 and F4 act like a molecular clamp on the planar heme molecule and are important in heme location. Amino acids at F8, E7 and B10 are important to ligands recognition and binding. However, amino acids at positions B9, B14, CD1, E10, and E11 have been clearly shown to play a role in ligand binding or in positioning of residues E7 and/or B10 residues (2).

The diversity in functionality of this Hbs is imparted by the residues at the distal site, and the heme group that serves as the ligand-binding site (4). As it is shown in Figure 1.2 the heme consist of an iron atom (Fe) coordinated by a heterocyclic ring, called porphyrin. This formed with the iron at the distal and proximal position in the heme pocket. Most of the time, the proximal HisF8 is bound to the Fe at the fifth coordination position. While ligands bind at all four nitrogen in the center of the ring, which lie in a plane. Two additional bonds can be

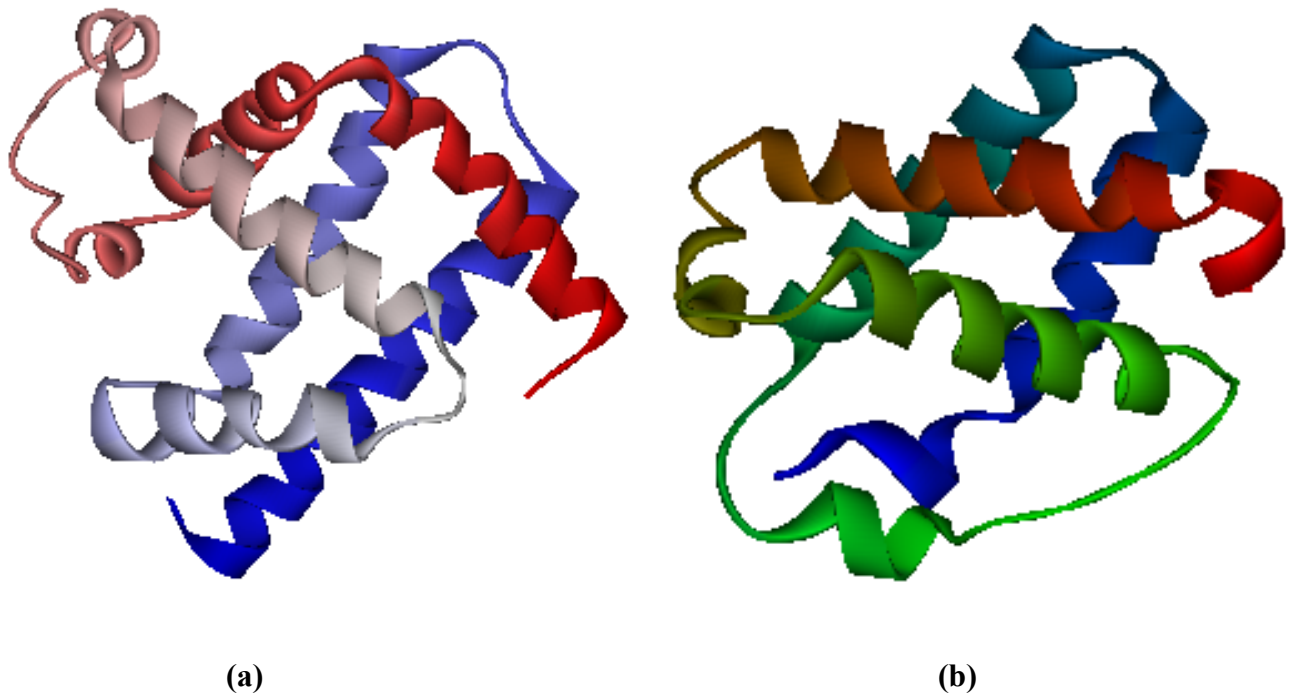


**Figure 1.1 Hemoglobins helical arrangement. (a) Three-over-three helical sandwich from horse heart myoglobin (PDB:1DWR). (b) Two-over-two helical sandwich from the protozoan *Paramecium caudatum*, trHbP (PDB:1DLW).**

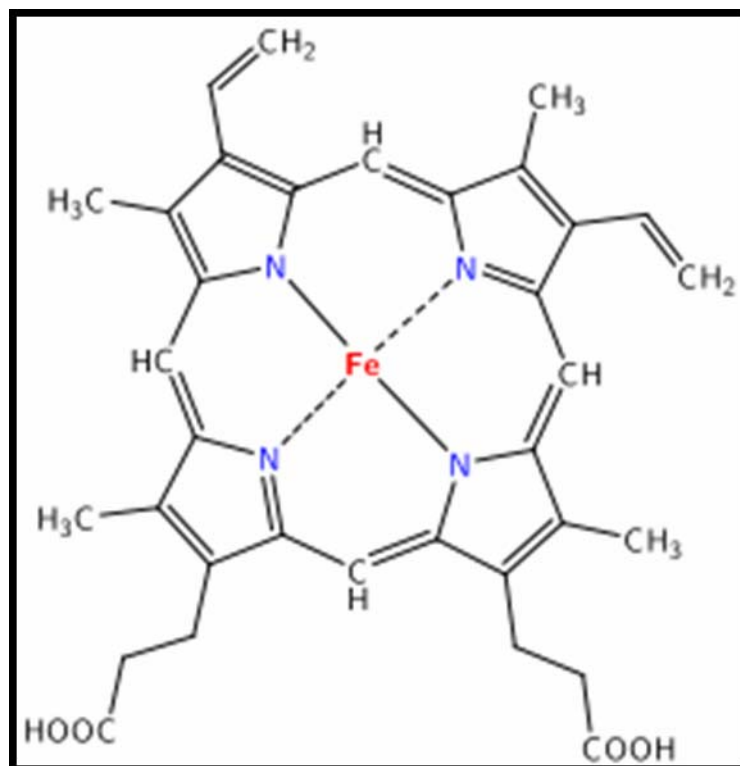


**Figure 1.2 Structure of the heme group, which consist of a porphyrin ring bound to an iron atom (red) in the center. This Fe has six coordination sites, where four are occupied by the nitrogen atoms (blue) of the porphyrin ring and the other two can be occupy by the ligand and histidine at the F8 position. Illustration from [www.wikipedia.com](http://www.wikipedia.com).**

formed with the iron at the distal and proximal position in the heme pocket. Most of the time, the proximal HisF8 is bound to the Fe at the fifth coordination position. While ligands bind at the sixth coordination position of the heme iron at the distal site. Usually, this binding site is located between the heme iron and E7 residue (1). Figure 1.3 shows the heme pocket of horse heart Mb-CO where the distal and proximal sites are labeled with (a) and (b), respectively. The black arrow shows the six coordination position, which can be occupied by the ligand. The orientation and binding stability is dependent on the nearby residues of the protein structure, and the oxidation state of the Fe atom ( $\text{Fe}^{2+}$  or  $\text{Fe}^{3+}$  state), which dictates whether the heme can bind a different ligand.

## 1.2 Spectroscopic characteristics of hemoglobin.

Hemoglobins are also attractive to study because of their optical properties and the presence of an iron atom at the prosthetic group (5). Several spectroscopic techniques have been used to determine structure and function of Hbs. For example, two of the techniques generally employed are: Ultraviolet- visible (UV-Vis) and infrared (IR) spectroscopy. The heme strongly absorbs light in the visible and near ultraviolet region of the electromagnetic spectrum. Figure 1.4 shows a typical ultra violet-visible (UV-Vis) spectrum of a heme porphyrin, Hemoglobin II from *Lucina pectinata*. The UV-Vis spectrum shows an intense band near the ultraviolet region, known as the Soret band, while a pair of weak bands between 500 and 600 nm are designated as the Q bands, also known as  $\alpha$  and  $\beta$ . The UV-Vis spectrum of hemoglobins was explained by the Gouterman *et al.* (7). In a few words, the porphyrin ring has one low unoccupied orbitals (LUMO)  $\pi^*$  with an  $e_g$  symmetry while has

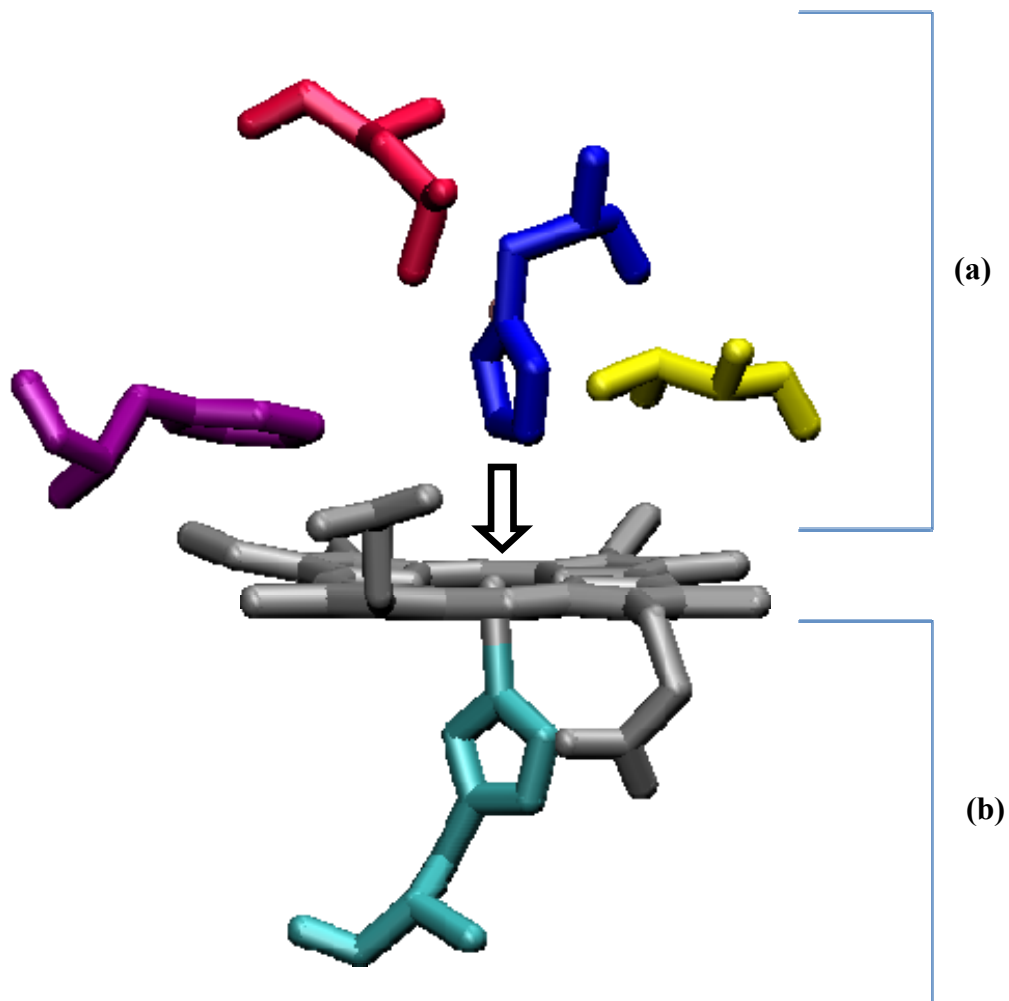


**Figure 1.3 Structure of the heme pocket from horse heart myoglobin (PDB:1DWR). The area designated as (a) and (b) correspond to the distal and the proximal site in the heme pocket, respectively. The heme group (gray) occupies the middle of the pocket. Residues in each of the sites are represented in different colors: ValE11(yellow), HisE7 (blue), LeuB10 (red), PheCD1 (purple) and His93 (turquoise). The ligand can occupy the sixth coordination position indicated by the black arrow. The drawings were made with VDM 1.8.5.**

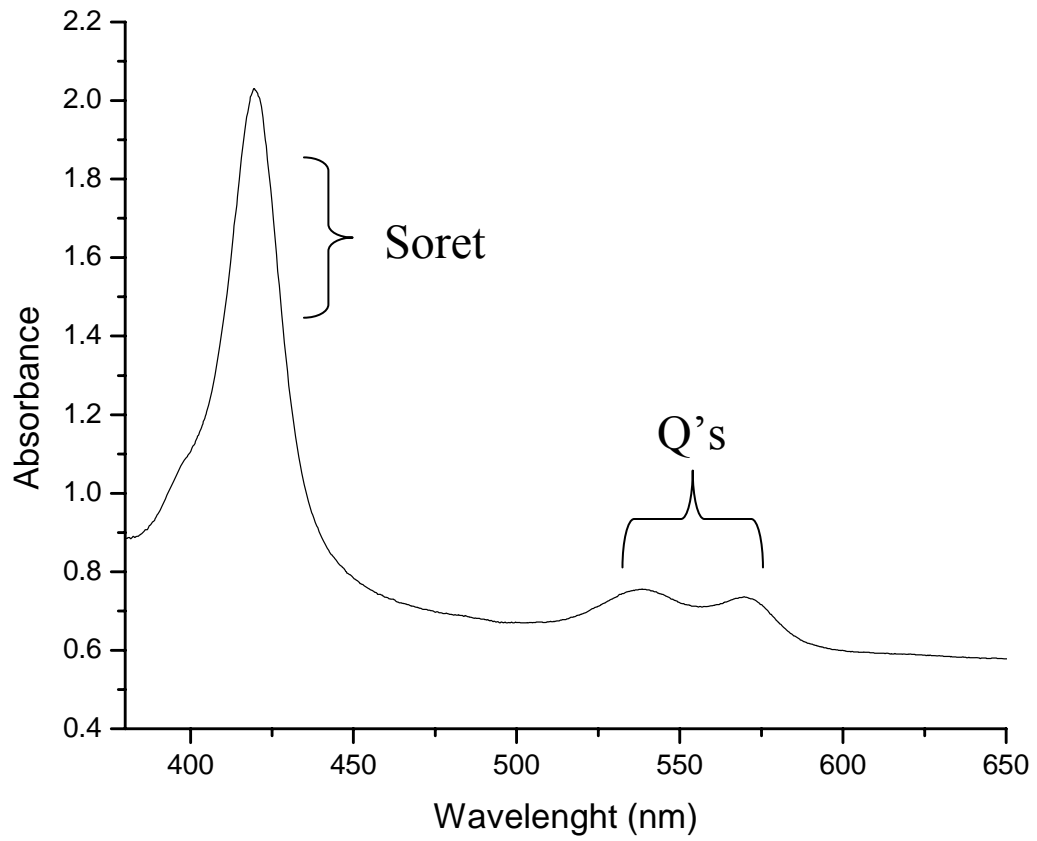


**Figure 1.4 UV-Vis spectra for heme protein, Hemoglobin II (HbII) from *Lucina pectinata*, which shows the characteristics Soret and Q's bands.**

two highest occupied orbitals (HOMO) with  $a_{1u}$  and  $a_{2u}$  symmetries. The Soret band is designated as high energy permitted transition from  $\pi$  to  $\pi^*$ , while the Q's band are unpermitted transition but through vibronic coupling and charge-transfer transitions they can borrow intensity from the higher energy transitions allowing the observation of these bands. The dipole transitions add up for the Soret, and nearly cancel for the weaker Q ones (7).

Infrared spectroscopy (IR) has been used for the study of protein structure due to the vibrational frequencies of the amino acids and ligand bound to the Fe which give information about bond length, angle, geometry and interactions (8). The characteristic vibrational frequencies of the amide I are used for the determination of the secondary structure of the protein (8,9). If the protein configuration is primarily  $\alpha$ -helix, the maximum frequency for the amide I will be approximately  $1653\text{-}1657\text{ cm}^{-1}$ . While for  $\beta$ -sheet it will be approximately  $1630\text{-}1635\text{ cm}^{-1}$ . These frequencies can change depending of the strength of hydrogen bonding between the C=O and the N-H in the  $\alpha$ -helix and the  $\beta$ -sheets. Also, the interaction of the side chains of some residues with ligand can be analyzed by IR because various functional groups absorb in this region and serve as a probe of chemical interactions between them. Small ligands that are attached to the heme iron absorb in the IR region, and offers information about the distal heme environment, which simultaneously offers information about its function. An important example of this is the carbon monoxide (CO) which is a widely used ligand for studying heme proteins because the presence of charged molecules around the CO produces marked changed in the IR spectrum (2,10,11).

### **1.3 Carbon monoxide as a probe of heme distal environment**

Carbon monoxide has been used widely as a vibrational probe of heme proteins to examine structure and bonding interactions, because of the variation in vibrational frequencies due to the influences of the heme environment (10). The stretching of CO ( $\nu_{\text{CO}}$ ) in gas phase is  $2143 \text{ cm}^{-1}$ , but when it is bound to heme, its decreases by approximately  $200 \text{ cm}^{-1}$  (2,10). The phenomenon of back-bonding between Fe-CO bond induces the  $\nu_{\text{CO}}$  reduction from the gas. Figure 1.5 shows the diagram describing the phenomenon of back-bonding which consist of two parts: (A) in which the carbon of the carbonyl donated two electrons to the vacant Fe d-orbital (designated as M in the diagram). This electron donation makes the Fe more electron rich, and in order to compensate this increased in electron density, the filled Fe  $d_{z^2}$  orbital interact with the empty  $\pi^*$  orbital on the CO ligand to relieve itself of the added electron density, as presented in Figure 1.5(B). This second part is called  $\pi$  back-bonding. This back-bonding interaction is disrupted by the nearby amino acids, especially at the B10, E7 and E11 position, in the heme center. The nearby amino acids can interact with the CO and its vibrational signal change as function of the electrostatic environment. An example of these is the case of mammalian Mb. In ferrous mammalian Mb various  $\nu_{\text{CO}}$  are observed, and they have been characterized (11) and assigned to different heme conformations or structural states. The three different structural states have been assigned in mammalian myoglobin: the  $A_0$  conformer with  $\nu_{\text{CO}}$  at  $\sim 1965 \text{ cm}^{-1}$ , the  $A_{1,2}$  with a  $\nu_{\text{CO}}$  at  $\sim 1945 \text{ cm}^{-1}$ , and the  $A_3$  with a  $\nu_{\text{CO}}$   $\sim 1932 \text{ cm}^{-1}$ . Figure 1.6 (a-c) shows a representation of the different conformations adopted by the heme distal site in mammalian Mb. Figure 1.6 (a) shows the  $A_0$  conformer that has been ascribed to a protonated His (at the

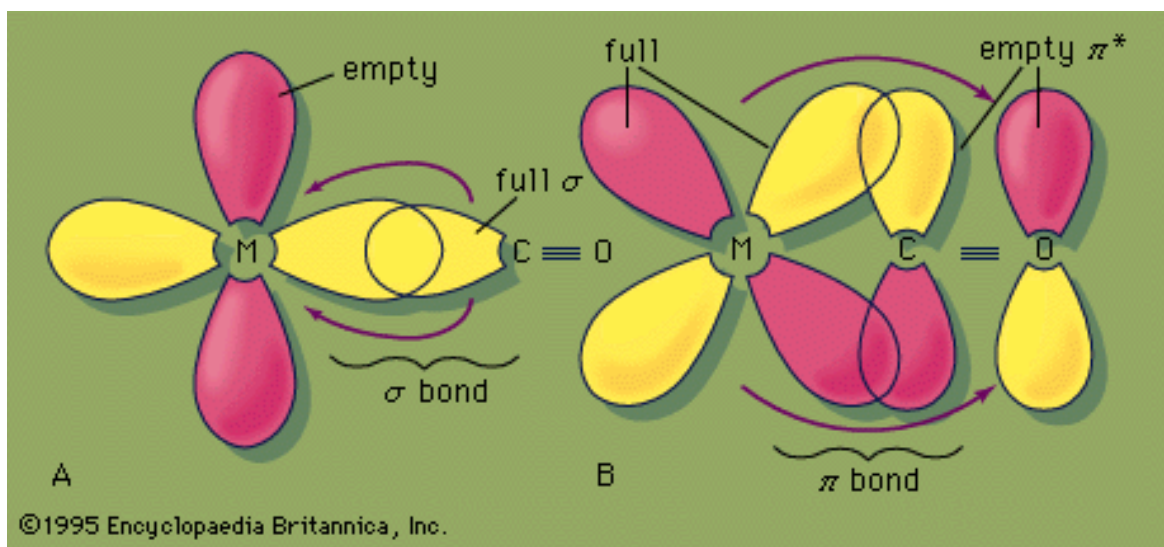


**Figure 1.5** Diagram describing the phenomenon of back-bonding which consist of two parts: (A) in which the carbon of the carbonyl donated two electrons to the vacant Fe d-orbital (Fe designated as M in the diagram), and (B) where the Fe compensate the increased in electron density of the CO electron donation, by interaction of the filled Fe  $d_{z^2}$  orbital with the empty  $\pi^*$  orbital on the CO ligand. Diagram from [www.encyclopediabritannica.com](http://www.encyclopediabritannica.com)



E7 position) adopting an open conformation with neither electronic nor hydrogen bonding interaction with the bound CO (11). Meanwhile, Figure 1.6 (b) presents the  $A_{1,2}$  conformer that has been assigned to a closed structure in which the His is unprotonated, having polar interactions with the bound CO. Lastly, Figure 1.6 (c) shows the closed conformation,  $A_3$ , in which the distal His is protonated having a hydrogen bond with the CO. These structural states are originated from effect of back-bonding produced by the electronic effects of the heme environment (11,12).

When a positive electric field is near the oxygen of the CO as in the case of the  $A_3$  conformer, the degree of back-bonding is enhanced, increasing the order of the Fe-C bond and decreasing the order of the C-O bond and  $\nu_{CO}$ . This allows the formation of another resonance structure compared to the one observed naturally (Figure 1.7 (a)). On the other hand, when there is a decrease of a positive electric field near the oxygen of the CO as in the  $A_0$  conformer, the order of the Fe-C bond decreases, and the order of the C-O bond and the  $\nu_{CO}$  increase. Therefore, an inverse correlation has been established between the  $\nu_{CO}$  and  $\nu_{Fe-C}$  as shown in Figure 1.8. Shaded symbols are obtained from wild type heme-proteins. The open symbols represent the mutant proteins. The wild type Mb (green triangle at line 2), showed a  $\nu_{CO}$  and  $\nu_{Fe-C}$  at 512 and 1944  $\text{cm}^{-1}$ , respectively. When the HisE7 is mutated to various non-polar residues, such as Leu or Phe, the data points move towards the lower right corner of the correlation line because the  $\nu_{Fe-C}$  frequency decreases and the  $\nu_{CO}$  frequency increases represented by the (empty green triangles at line 2) which indicate a close conformation and low electrostatic interaction of the residues and CO. The data point for

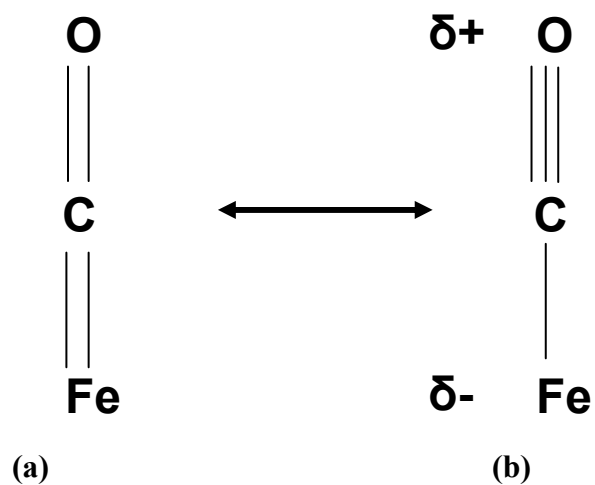


**Figure 1.7 Representation of the resonance structures adopted when the CO is bound to Fe (b). When there is a positive electric field around the oxygen; presence of back- state; where, the electrons in the  $d\pi$  orbital of  $\text{Fe}^{+2}$  are donated to the  $\pi^*$  orbital of the CO as is bonding and the resonance structure (a) is stabilized. Diagram modified from reference 2.**

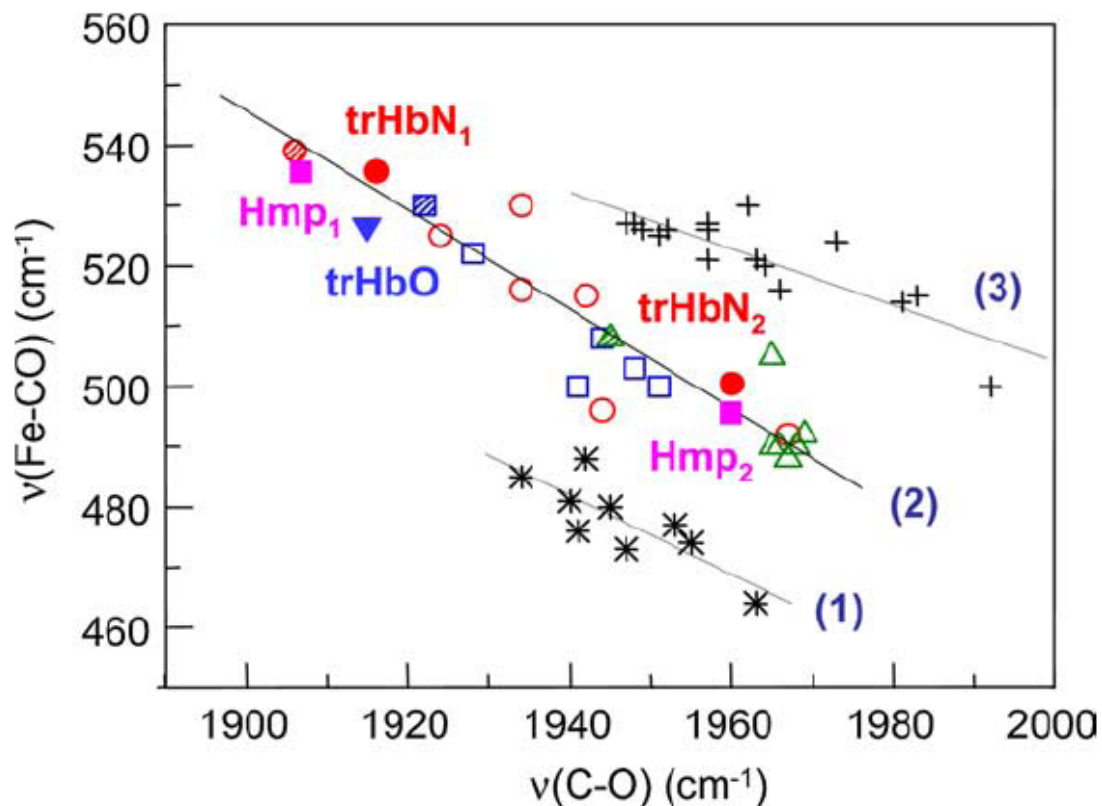
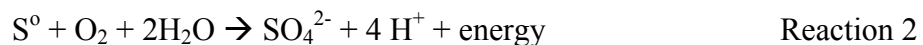


Figure 1.8 Inverse correlation diagram of the Fe–CO stretching frequency and the C–O stretching frequency for a variety of heme proteins and porphyrin derivatives. Line (2) is for complexes in which the proximal ligand is a histidine. The shaded figures are for the wild type protein: horseradish peroxidase (●), cytochrome c peroxidase (■) and myoglobin (▲). The corresponding open figures are obtained from their mutant proteins. Figure from reference 2.

horseradish peroxidase, HRP, (shade circle at line 2) is located in the upper left corner of the correlation line because the CO bound is stabilized by hydrogen bonds. Similar to HRP, the point for cytochrome c peroxidase (CCP) is also located at the upper left corner of the correlation line, which indicates the presence of a close conformation due to the strong electrostatic interactions of the residues and the CO. When the polarity of the distal environment is reduced, the data points shift to the lower right corner, which indicate a decrease of hydrogen bond interactions. Low  $\nu_{\text{CO}}$  indicates a closed structure, while higher  $\nu_{\text{CO}}$  designates to an open structure made between nearby residues and the bound CO.

#### **1.4 Hemoglobin from *Lucina pectinata***

During these past decades, comparisons between models of vertebrates and invertebrates hemoglobins make possible the elucidation of structure-function and dynamic relation and behavior of heme proteins. Good models for ideal invertebrate hemoglobin are the hemoglobins found in *Lucina pectinata* (*L. pectinata*). This clam is an intriguing invertebrate organism characterized by the presence of highly concentrated hemoglobins (13). The bivalve mollusk lives in sulfide-rich mangroves of the southwest coast of Puerto Rico, and houses intracellular chemoautotrophic symbiotic bacteria that need to be supplied with oxygen and hydrogen sulfide ( $\text{H}_2\text{S}$ ). *L. pectinata* has three hemoglobins: HbI, HbII and HbIII. These Hbs supplies the bacteria with  $\text{O}_2$  and  $\text{H}_2\text{S}$ , the former HbI transports the  $\text{H}_2\text{S}$  to the bacteria, while HbII and HbIII deliver the  $\text{O}_2$ . It has been suggested that the  $\text{H}_2\text{S}$  is oxidized as presented in Reaction 1 and 2. The energy produced by these reactions is used by the bacteria to fix carbon dioxide and produce the necessary nutrients.



HbI is a monomeric protein that binds and transports H<sub>2</sub>S, a toxic gas, to the bacteria, is one of the few known hemoglobins that carries H<sub>2</sub>S in its heme active site. Recently studies had demonstrated that H<sub>2</sub>S is synthesized endogenously in mammalian tissue and may function as a neuromodulator (14, 15). Crystal structure analysis (16) and the cDNA-derived amino acid sequence (17) of the monomeric HbI have demonstrated that the distal heme pocket contains a distinctive structural organization involving a glutamine residue (Gln) and three phenylalanine (Phe) at positions E7, B10, CD1 and E11, respectively, as it is shown in Figure 1.9.

Previous spectroscopic studies have shown that the unique sulfide binding and stabilization properties of HbI seem to be dictated by these atypical distal amino acids (18). According to <sup>1</sup>H-NMR studies, the orientation of the GlnE7 changes to stabilize the bound ligand. Figure 1.10 (a) shows that in the met-cyano and O<sub>2</sub> complexes the amine group of the Gln has been suggested to serve as a hydrogen bond donor (19). As shown in Figure 1.10 (b), the met-aquo and H<sub>2</sub>S complexes, the carbonyl group of the GlnE7 serves as a hydrogen bond acceptor. An iron-sulfide mechanism has been postulated which involves an unique orientation of the 2-vinyl groups and a rocking freedom of the heme, due to the lack of hydrogen bonds or strong polar interactions between the propionates and the polypeptides (20,21). Previous FT-IR analysis on the wild type HbI-CO complex indicated that three CO stretching frequencies at ~ 1936 cm<sup>-1</sup>, 1950 cm<sup>-1</sup> and 1960 cm<sup>-1</sup> dominated its vibrational

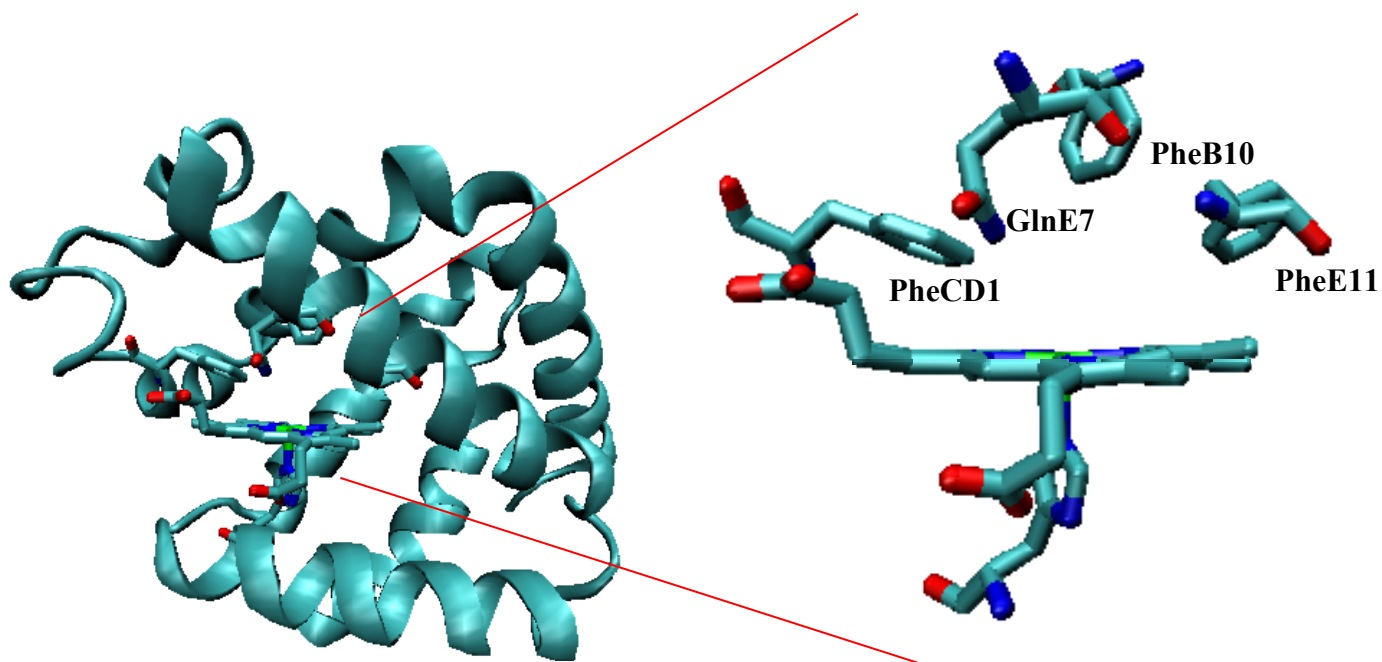


**Figure 1.9** Distal heme pocket of met-aquo HbI from *Lucina pectinata* (PDB: FLP). The residues at the distal position are identified by a three letter abbreviation and the corresponding position. The drawings were made with VDM 1.8.5.

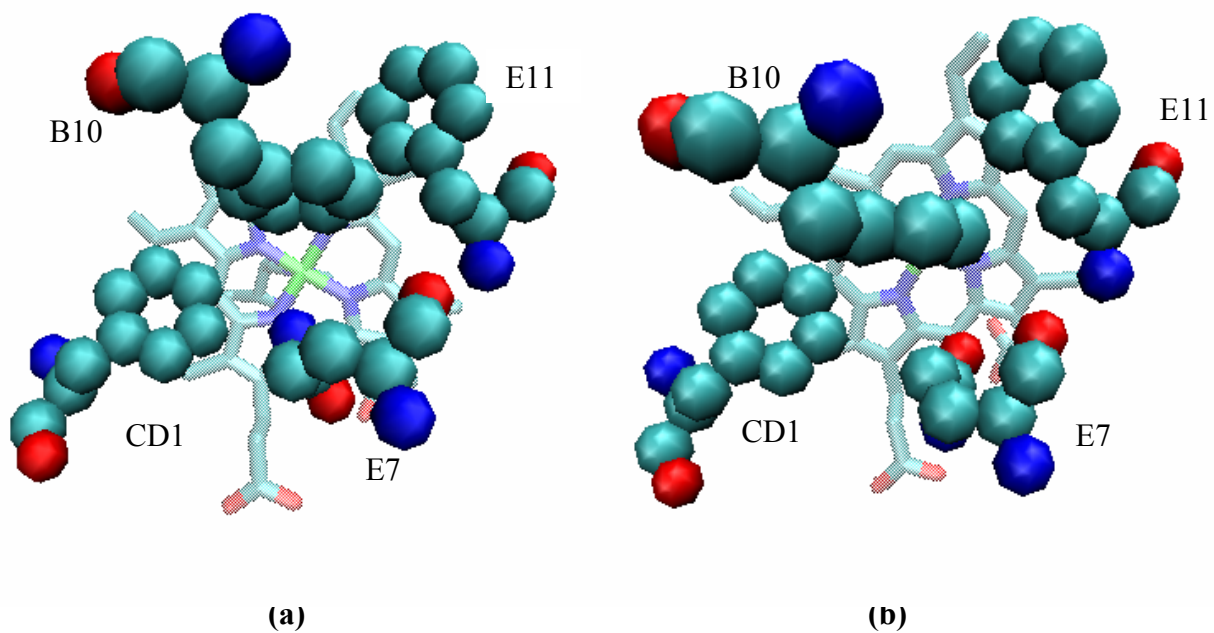


**Figure 1.10** The structures of (a) ferric HbI and (b) HbI-H<sub>2</sub>S complexes. The view from the top of the heme showed the displacement of the distal heme residues (GlnE7 and PheB10). The drawings were made with VDM 1.8.5.

spectrum. The main  $\nu_{\text{CO}}$  at  $1936\text{ cm}^{-1}$  was ascribed to the highest populated  $A_3$  conformer in which a synergistic effect between the GlnE7 and the PheB10 and PheE11 residues created a strong positive electrostatic environment around the bound ligand in a so called closed cage configuration. A direct hydrogen bonding of the GlnE7 and the bound CO as well as multipolar interaction of the Phe residues with the ligand was suggested. The very small  $\nu_{\text{CO}}$  at  $1950\text{ cm}^{-1}$  was assigned to the lowest populated conformer  $A_{1,2}$  in which only the GlnE7 was responsible for generating a weaker hydrogen bonding ( or polar) interaction with CO in a direct closed configuration. The presence of the  $\nu_{\text{CO}}$  at  $1960\text{ cm}^{-1}$  was designated to the lost of a positive electrostatic environment surrounding the bound ligand which in turn generates an open  $A_0$  conformer (22). Studies with rHbI and mutants at the B10 and E7 positions had demonstrated that the flexibility of the HbI distal site is dictated mainly by GlnE7. However, the presence of multiple conformers in the wild type ferrous CO derivative is evidence that reflects the overall flexibility of the HbI distal pocket. In this system, the closed cage configuration predominates, indicating that both GlnE7 and PheB10 are closed enough to interact with the bound CO thus controlling ligand reactivity (23). According to recent studies, residues at B10, E7, E11 and E14 are very important in regulating the binding and discrimination of ligands (2). Truncated hemoglobin I (trHbN) from *M. tuberculosis* have a TyrB10, LeuE7 and GlnE11 residues at the distal heme environment. Results of Resonance Raman on mutants at different position and crystallographic data of dioxygen trHbN suggest that a hydrogen bonding network between the TyrB10, GlnE11 and the bonded oxygen stabilize the ligand (2). Our FT-IR results for HbI suggest that CO is hydrogen bonded to

GlnE7 distal amino acid and a synergistic action of the three Phe, accounts for the low  $\nu_{\text{CO}}$  frequencies of the A<sub>3</sub> conformer. The aromatic nature of the heme pocket of HbI is the main contribution to the observed conformers and ligand-binding properties.

### **1.5 Objective**

Despite all previous work, the role of the phenylalanine (Phe) in the position E11 in heme proteins is not well understood. It has been suggested that this E11 amino acid is involved in the functionality, structural dynamics, and ligand migration (2, 3, 11). Here, we will use HbI from *Lucina pectinata* as a model. Site-directed mutagenesis and CO complex with these proteins, together with FT-IR and kinetics studies were performed to elucidate the role of the E11 in the distal heme environment of HbI.

## 2 MATERIALS AND METHODS

### 2.1 Cloning of the HbI mutants

Cloning, expression, lysis and purification are the procedures that have to be performed to generate a representative sample of a specific recombinant protein. Site-directed mutagenesis and the expression of various HbI mutants provided an approach to study the relationship between structure, function and dynamics of the distal heme pocket of wt-HbI. With this technique as a template, we are able to generate various mutants at different positions. Therefore, in our experiments, we selected the substitution of the amino acid at E11 position to unveil its possible role on ligand stabilization and ligand dynamic control. The construction of the HbI PheE11Gln, HbI PheE11Val and PheE11Tyr were performed according to the procedure presented in literature (24). Unique *E. coli* Bli5 competent cells with the plasmid (corresponding to each HbI mutant at the E11 position) were developed at the Biomolecular Laboratory of Dr. Carmen Cadilla (U.P.R.- Medical School, Río Piedras), and provided in scraped Petri dishes. To enhance the life period of the competent cells, they were stored as a “frozen stocks”, a mode of storage media at low temperature (-80°C) by adding sterilized glycerol.

### 2.2 Large- scale expression or fermentation of the HbI mutants

The large scale expression or the fermentation protocol for each mutant was done as described previously (24) with a few modifications, and require at least two days of pre-work. Initially, the equipment and glassware used for the fermentation process was cleaned and

sterilized (Market Forge, Sterilmatic). The following solutions were prepared: 250 mL of 50% w/v glucose (Fisher), 500 mL of 1.5 M monobasic potassium phosphate ( $\text{KH}_2\text{PO}_4$ , Fisher), 500 mL of 30% v/v ammonium hydroxide ( $\text{NH}_4\text{OH}$ , Fisher), 5 mL of 1mM IPTG (Sigma), 500 mL of Terrific Broth (TB) medium (EZ-Mix, Sigma) with 30  $\mu\text{g}/\text{mL}$  of chloroamphenicol (Fisher) and 70  $\mu\text{g}/\text{mL}$  of kanamycin (Fisher), and 500mL containing 0.17 M  $\text{KH}_2\text{PO}_4$  (Fisher) and 0.72 M  $\text{K}_2\text{HPO}_4$  (Fisher). All the solutions were sterilized for 20 min at 120°C with the exception of 30% v/v  $\text{NH}_4\text{OH}$ .

One day before fermentation, cells from a frozen stock were grown in a 250 mL sterilized Erlenmeyer containing 50 mL of the TB medium. The culture was incubated for 12 hours in a shaker (PRECISION Reciprocal Shaking Bath) at 120-150 rpm, and 37 °C. After 12 hours, the culture was transferred to a 2500 mL culture flask with the 450 mL of the TB medium, and incubated overnight (12 hours) in a shaker at 120-150 rpm and 37 °C. The large-scale expression of all the HbI mutants was performed using a Bioflo 110 Modular Benchtop Fermentator. The 4 L TB media for the large-expression was prepared directly inside the fermentator vessel. The water jacket was filled and the vessel sealed completely except for the exhaust which will have a 0.20  $\mu\text{m}$  filter and covered to avoid contamination with foil paper. The sealed vessel was placed inside the Sanyo Labo Autoclave and sterilized for 60 min at 121 °C.

After 12 hours, the vessel was removed from the autoclave, and placed in the BioFlo stirring base. The hoses and temperature probe were connected to lower the temperature in the vessel according to the fermentator manual (25). When the media reached a temperature

between 40 to 37 °C, 30 µg/mL of chloramphenicol (Fisher), 70 µg/mL of kanamycin (Fisher), 500 µL of antifoam solution (Sigma), sterile solution of 0.17 M KH<sub>2</sub>PO<sub>4</sub> and 0.72 M K<sub>2</sub>HPO<sub>4</sub>, 75 mL of the glucose (50% w/v) were added. When the temperature reached 37 °C, the pH and dissolved oxygen (dO<sub>2</sub>) sensor were introduced and calibrated inside the vessel following the instructions in the fermentator manual (25). Before inoculating (addition of the cell culture), a 25 mL aliquot of this media was collected to be use as blank for the measurement of optical density at 600 nm (OD<sub>600</sub>). This measurement was taken to monitor the cell growth along the procedure. The OD<sub>600</sub> was monitored using a UV-Vis Scanning Spectrophotometer SHIMADZU (UV-2101 PC Double Beam) equipped with the UV-probe software. After all these conditions were set, the media was inoculated with the overnight culture (prepared one day before the fermentation), and the other half volume of the glucose solution was added. At this time, approximately 3 mL of the inoculated media was collected using the vessel sample extraction port and the OD<sub>600</sub> was measured. To monitored cell growth, the OD<sub>600</sub> was measured every 30 minutes. When the a value of OD<sub>600</sub> was between 1 or 2, protein expression was induced by adding 5 mL of 1 M IPTG solution and 33 mg/mL hemin chloride in NH<sub>4</sub>OH (concentrate). The OD<sub>600</sub> was taken every 30 minutes after the induction until the lag phase was reached. Figure 2.1 shows an example of the bacterial growth of the Hbl PheE11Val as function of time. It follows a classical bacterial growth, having three phases: adaptation phase, logarithmic growth phase (log phase), and death phase (lag phase). The expression process was finished when two or three constant values of OD<sub>600</sub> reading were obtained in the lag phase. Then, the culture was collected in 500 mL centrifuge

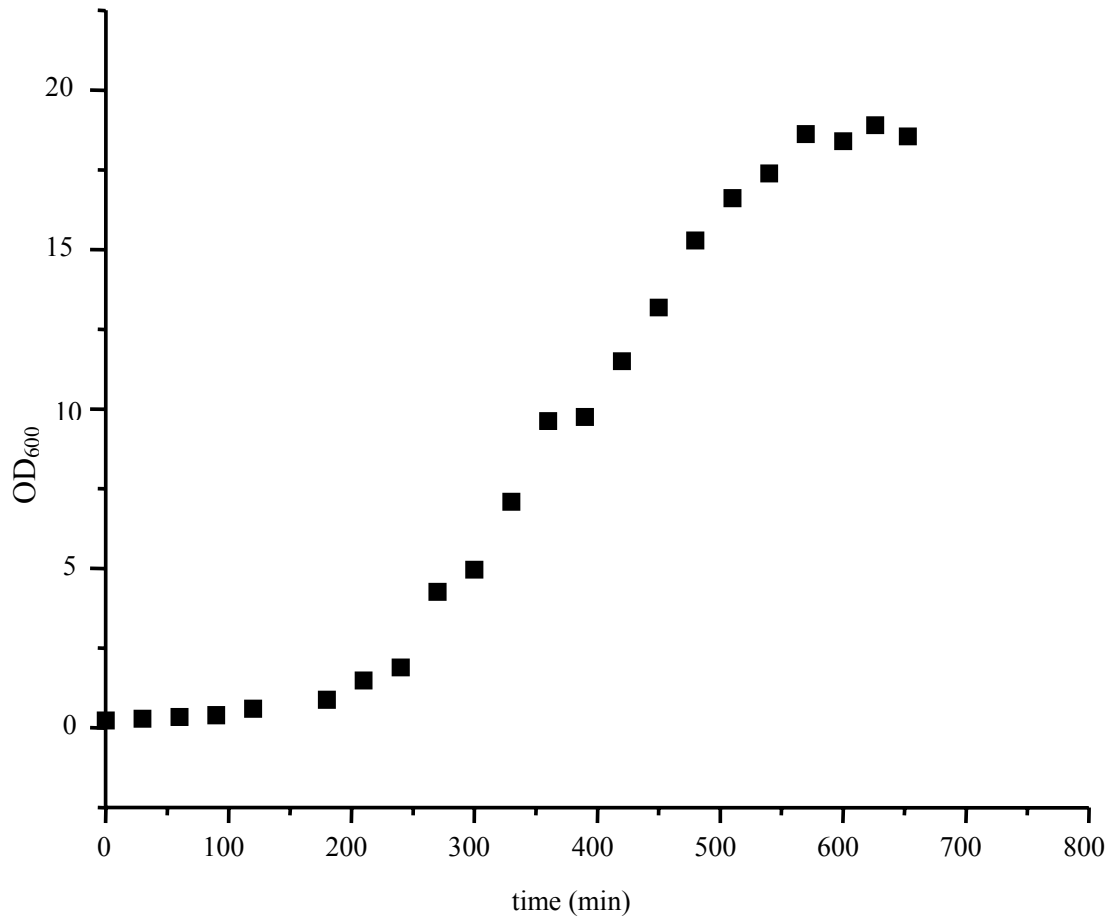


**Figure 2.1** Logarithmic bacterial growth curve of the HbI PheE11Val expressed with *E. coli* competent cells. Each point represents an absorption measure on a 30 minutes interval. This curve followed a classical bacterial growth.

bottle (Beckman) while the media was continually supplemented with oxygen to avoid the premature death of the bacterias, and a positive pressure was maintained inside the vessel to help the sample extraction transfer. The bottled culture was centrifuged for 20 minutes at 4,000 rpm at a temperature of 4 °C in a Beckman J2-HS Centrifuge. The supernatant were decanted from the precipitate or pellet. Then, the pellet was stored at -56°C for further lysis and purification procedures. Observations were taken describing the pigmentation and appearance of the pellet.

### **2.3 Bacterial lysis and heme protein isolation**

To isolate the protein from the bacterial cytoplasm, the cells membrane was broken by lysis. The pellet obtained was weighed to determine the amount of lysozyme and volume of buffer to be used. The lysate was kept on the ice all the time to inhibit any possible proteolytic activity. At the same time, two liters of Native Binding Buffer (NBB) with 58 mM dibasic sodium phosphate ( $\text{Na}_2\text{HPO}_4$ , Fisher), 17 mM monobasic sodium phosphate ( $\text{NaH}_2\text{PO}_4$ , Fisher), and 68 mM sodium chloride ( $\text{NaCl}$ , Fisher) was prepared and sterilized for 25 min at 120 °C. The pellet was resuspended in approximately 90 mL of NBB per 35 g of bacteria. While, one mg lysozyme (Sigma) / g bacterium was added to the resuspended pellet. Once the lysozyme was added, it was incubated on ice for 45 minutes; sporadically watching and mixing the solution until an extremely viscous solution was formed. To avoid the degrading of the protein, 20  $\mu\text{L}$  of protease inhibitor cocktail (Sigma) was added for approximately every 100 mL of NBB. The lysate was sonicated five times, for 1 minute and 15 seconds at 25% intensity, each with one minute of rest between each step. After sonication, the lysate

appeared completely aqueous without the viscous aspect. The lysate was centrifuged at 18,000 rpm at 4 °C for an hour. At this time, the supernatant was collected and purged with carbon monoxide gas (CO) for 30 min with constant agitation. The sample was stored (at -56 °C) to be further purified. Volume, appearance and other observations were documented for further references.

## **2.4 Purification of the HbI mutants**

Several chromatographic procedures were employed for the hemoglobin and protein separations using different resins and elution conditions. The entire process of purification of the HbI mutants involves: affinity chromatography, and size exclusion chromatography. All of these purification procedures were performed on a Fast Performance Liquid Chromatography system (ÄKTA FPLC, Amersham Bioscience) equipped with a Frac-950 fraction collector, and an UV-Vis lamp which helps monitoring the elution fraction from the column at 280 nm and presents an elution histogram of the run. At the same time, other parameters, such as: temperatures, conductivity, among others, were recorded with the software UNICORN<sup>®</sup> 4.0.

### **2.4.1 Affinity Chromatography**

Affinity chromatography was carried out using a metal affinity resin, BD Talon<sup>™</sup> (Clontech). This resin contains a sepharose bead bearing the tetradentate chelator of cobalt (II) which binds polyhistidine-tagged recombinant proteins. This resin is highly selective towards polyhistidine-tagged proteins, therefore, offering high yields of our expressed protein. The lysate was centrifuged at 18000 rpm at 4°C for 30 minute to eliminate all the

impurities left in the previous step. The supernatant was collected and filtered with a 0.45  $\mu\text{m}$  syringe filter (Fisher). A Tricorn 10/100 column (Amersham Bioscience) was packed with BD Talon<sup>TM</sup> Resin following the manual instructions (26). This column contains  $\sim$  8-10 mL of the resin which is equivalent to one bed volume (BV). Once the column was completely packed, it was equilibrated with 10 BV of the equilibrating buffer (50 mM sodium phosphate, 300 mM sodium chloride, pH 7.0) at a flow rate of 5.0 mL/min. Once the column was equilibrated, 20 mL of the lysate was loaded into the column at a flow rate of 1.0 mL/min. The resin was washed using a buffer (50 mM sodium phosphate, 300 mM sodium chloride, and 10 mM imidazole at pH 7.0). This wash buffer was used to remove all the other proteins that are weakly attached to the resin. For the complete elution of the HbI mutants, a buffer was added (50 mM sodium phosphate, 300 mM sodium chloride, and 150 mM imidazole at pH 7.0). The eluent, with a red color, was collected in the Frac-950 fraction collector. The fractions were collected based on the elution chromatogram recorded in the software UNICORN<sup>®</sup> 4.0. Figure 2.2 shows the elution profile for the affinity chromatography of HbI PheE11Val which contains two main bands. The first band was assigned to impurities and the second to a mixture of the protein of interest and salts.

This procedure was followed for the other: HbI PheE11Val, PheE11Tyr, and HbI PheE11Glns. After this, the imidazole must be completely removed from the protein to ensure the protein functionality. Then, the collected samples were concentrated using an AMICON ultra- filtration cell with YM-10 membranes; and at the same time the solvent was washed out with deionized water for storage (at  $-56\text{ }^{\circ}\text{C}$ ); until further purification.

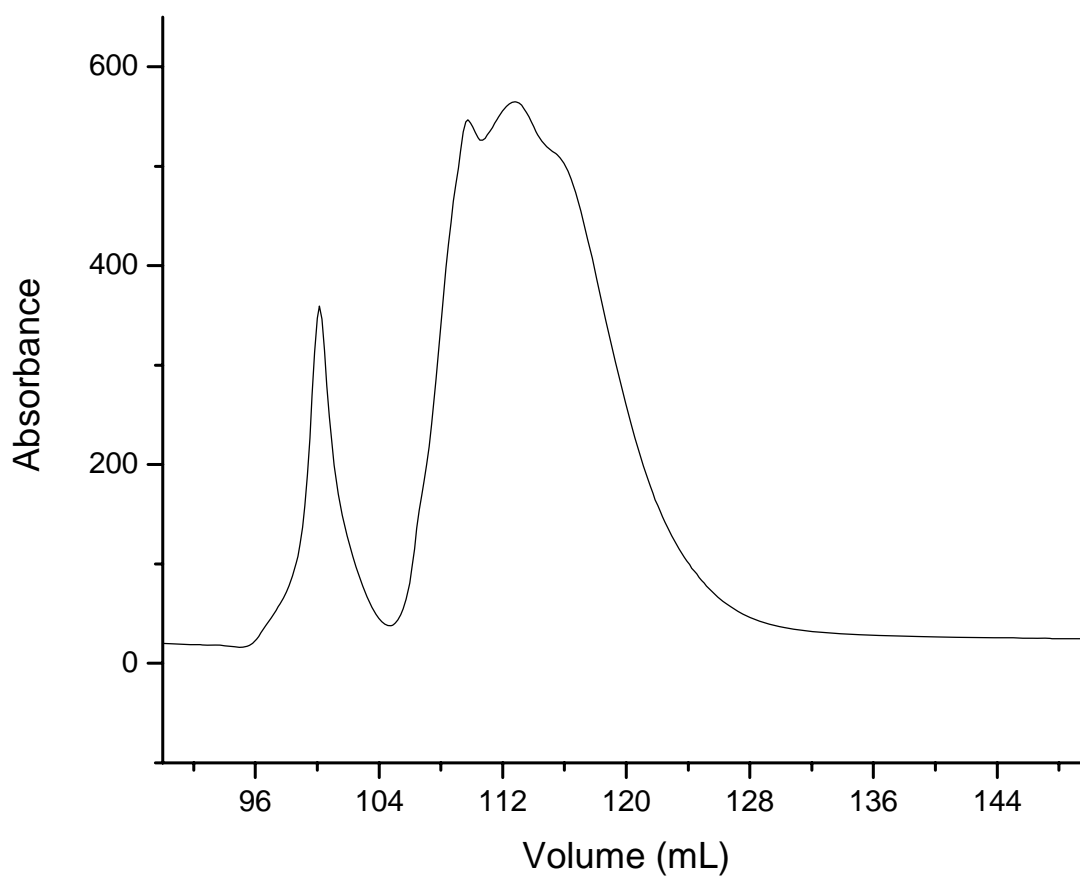


**Figure 2.2 Elution profile of the metal affinity chromatography used to separate HbI PheE11Val from impurities. The first peak at ~ 100 mL was assigned as impurities. The second major peak was assigned as a mixture of salts (imidazole) and our protein.**

#### 2.4.2 Size Exclusion Chromatography (SEC)

To complete the purification of the HbI mutants, we began with a HiLoad 26/60 Superdex 200 prep grade (Amersham Pharmacia Biotech) column with 26 x 60 cm dimension on an ÄKTA FPLC. This column was equilibrated with a buffer (50 mM sodium phosphate and 300 mM sodium chloride buffer at a pH of 7.0) at a flow rate of 2.0 mL/min. Approximately 5 mL of the concentrated protein was loaded onto the column using a flow rate of 4.4 mL/min making sure that the pressure does not exceed 0.3 MPa, and performed at room temperature. The eluted flow was collected in the fraction collector (Frac-950, Amersham Pharmacia Biotech). The process was monitored using the equipment software, UNICORN<sup>®</sup> 4, which recorded the elution chromatogram, which was used to determine which fractions contain our proteins. Figure 2.3 shows the elution profile completed with the FPLC procedure by monitoring the absorbance and the conductivity of the eluent. The solid line represents the effluent absorbance measurement at 280 nm as function of eluted volume. It only shows one main peak which correspond to the recombinant protein and a “bump” that was assigned the presence of imidazole that was eliminated using the AMICON ultra-filtration cell. It can also be observed the effluent in terms conductivity (dash line) were the main valley was assigned as a mixture of salts and impurities. These two peaks do not overlap which is evidence of a good purification process. The sample collected has the characteristic red color which, *a priori*, tells us that it is the protein of interest. In order to characterized and determine the oxidation state of sample an optical absorption spectrum of the fractions believed to contain the proteins was recorded using a UV-Vis. A classic met-

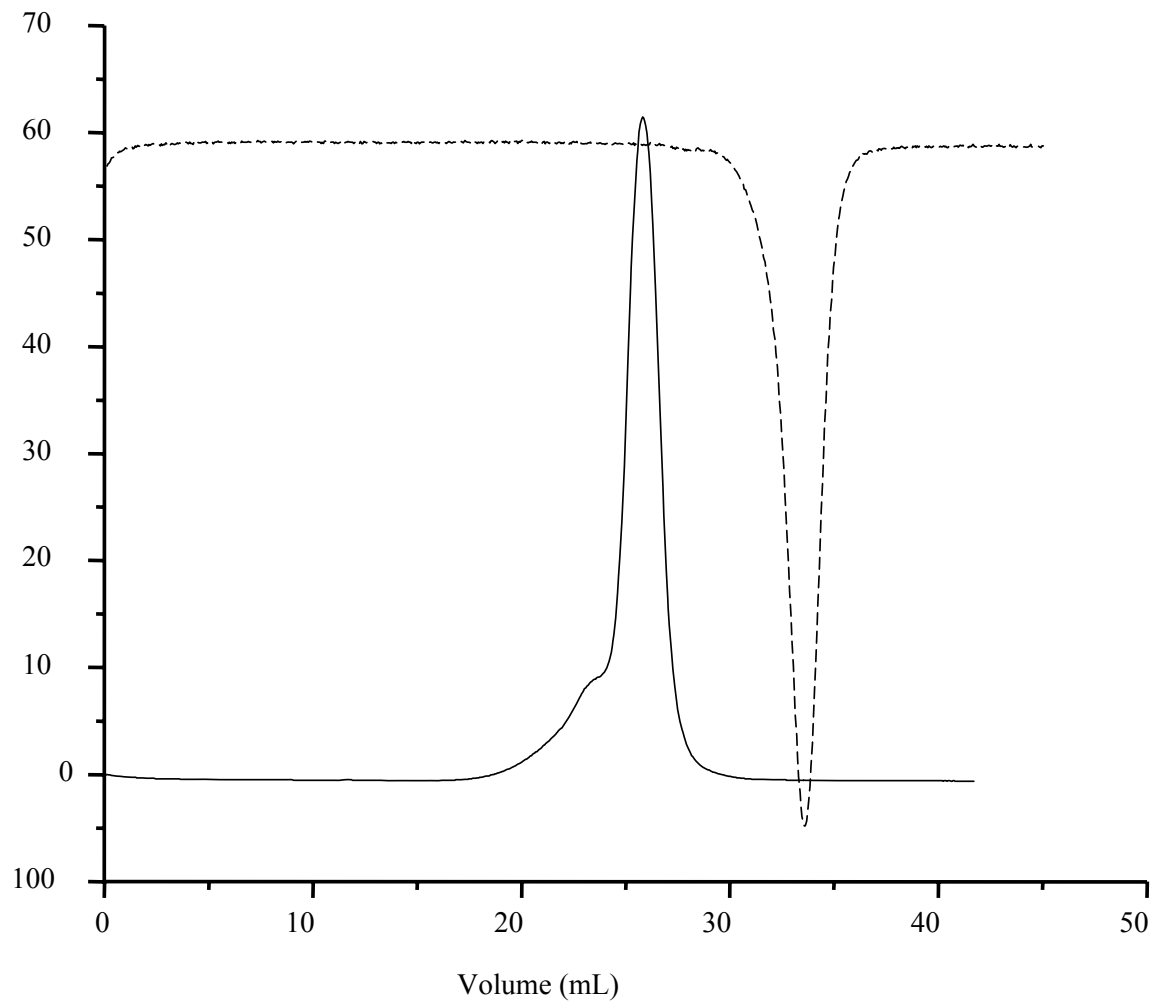


**Figure 2.3 The Size Exclusion Chromatogram of HbI PheE11Val. The protein elution profile using the UV lamp at 280 nm is represented by (—), and the the % conductivity elution profile of the effluent is shown (- - -) The “bump” observed in the (—) is due to the presence of imidazole during the process.**

aquo hemoglobin spectrum was obtained with a maximum absorbance at 407 nm and two Q bands at 502 nm and 633 nm.

## **2.5 Purity of the HbI mutants by SDS-PAGE**

To verify the quality of separation obtained by FPLC, the purity, and the process of HbI mutant's purification as well, a sodium dodecyl sulfate polyacrylamide gel electrophoresis (SDS-PAGE) was used. It separates proteins by charge using a discontinuous polyacrylamide gel as a support medium and sodium dodecyl sulfate (SDS) to denature the proteins. In general, the electrophoresis process consists of migration of proteins as a function of an electric field. The high molecular weight samples will remain at the top of the gel while proteins of low molecular weight will migrate to the bottom of the gel. The process is stopped before the proteins migrate to the bottom of the gel. The bands on the gel were compared with a prestained SDS-Page Standard (Bio-Rad) with a molecular weight range of 194,239 to 6,900 Daltons. This standard provides an easy way to assess the quality of an electrophoretic process, and makes it possible to monitor the separation of the protein.

The HbI mutant's samples were analyzed using SDS-PAGE and a stack of 8-16% Tris-HCl Ready Gels (Bio-Rad). First, a 20  $\mu$ L aliquot of SDS-Page Standard (Bio-Rad) was added to an Ependorf and it was heated at 32  $^{\circ}$ C for one minute. Second, a 20  $\mu$ L aliquot of the sample at each step of the purification procedure was taken and added to a different Ependorf. Then 10  $\mu$ L of the "running buffer" (1X -Tris, Glycine, SDS) was added to each sample and mixed in a VORTEX. Each sample was heated at 95  $^{\circ}$ C for 5 minutes on a sand bath. After this, 16  $\mu$ L of the samples were injected into the gel. The samples migrated

across the gel by applying a constant voltage of ~ 150 V, a current of ~114 mA was applied for a period of 45 minutes using a BIO-RAD power supply PAC 3000. Following the 45 minutes, the gel was removed from the system and dyed with Coomassie Blue G-250 for 15 minutes and washed out three times with a 10% acetic acid solution. Then, the gel was placed in deionized water overnight. The next day, the bands in the gel were compared with the standard. Figure 2.4 shows a SDS-PAGE for the HbI mutants and the different the purification steps. Lines 6, 9 and 10 are samples after the first purification method using affinity chromatography (Talon™) in which various mark appeared. While, the lines 7 and 8 presents the sample after desalting where several marks dissapeared . Once the sample was change to water, it was purified using SEC, lines 2 to 4. After all the purification procedure the sample in the gel have to present just one mark as presented in line 5. In the gel, we can observe all the purification steps completed for all the HbI mutants at the E11 position.

## 2.6 Concentration – UV-VIS of the HbI mutants

During the preparation of the samples, the concentrations and formation of the complexes were verified using their absorption spectrum. Figure 2.5 shows the UV-Vis spectrum for the met-aquo (·····), deoxy (----), and carbon monoxide (—) HbI derivatives. The hemoglobin concentration and formation of each complex (deoxy and carbon monoxide) was verified using the absorption spectral properties, and using the Beer-Lambert Law:

$$A = bc\epsilon \quad \text{Equation 1}$$

where A is the absorbance at the maximum wavelength ( $\lambda_{\text{max}}$ ) at the Soret band, b is the pathlength of the cuvette, c is the concentration of the sample and  $\epsilon$  is the absorptivity

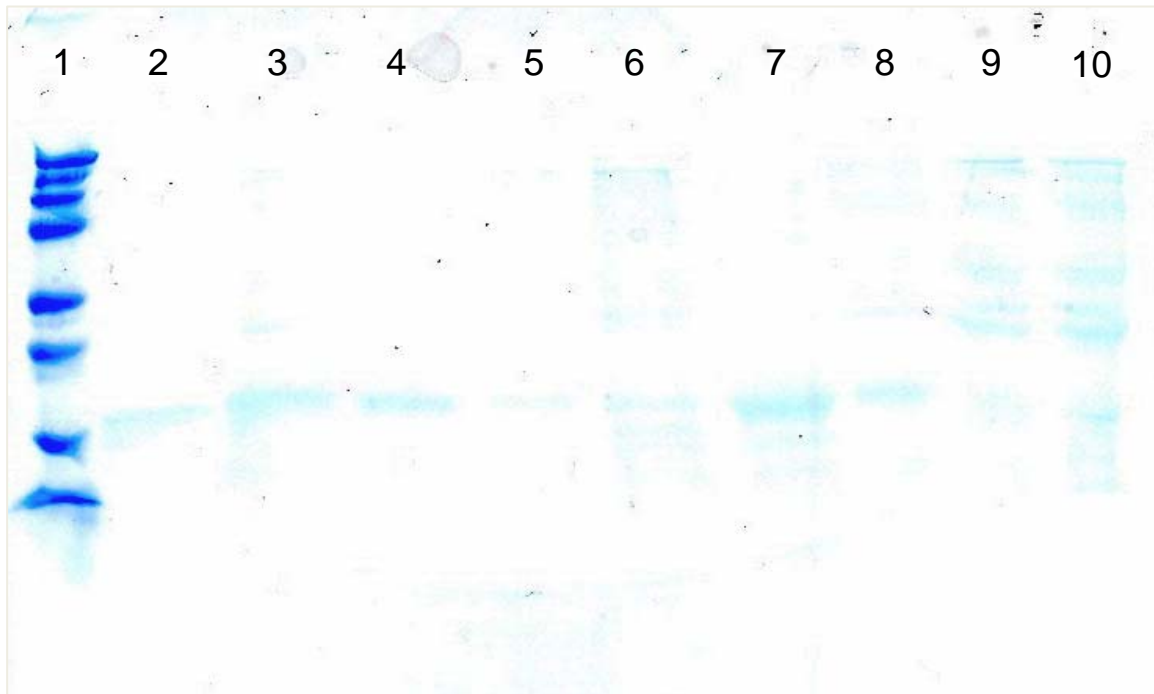


**Figure 2.4 SDS- PAGE for some of the HbI mutant at the E11 position. (1) SDS-Page Standard (2) rHbI after SEC (3) HbI PheE11Tyr after SEC (4) HbI PheE11Val after SEC (5) HbI PheE11Val after all the procedure of purification (6) HbI PheE11Tyr after BD Talon™ (7) HbI PheE11Tyr after desalting (8) HbI PheE11Val after desalting using FPLC (9) HbI PheE11Val after BD Talon™ (10) HbI PheE11Gln after BD Talon™.**

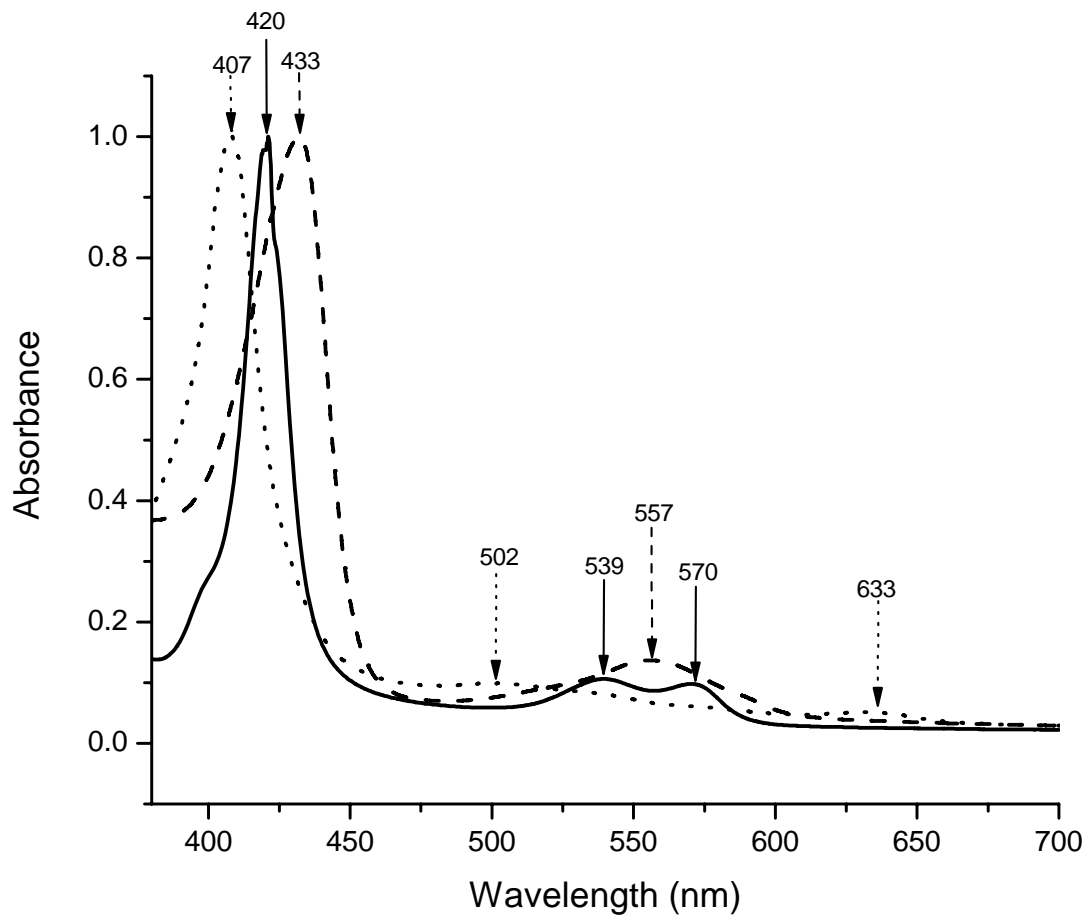


**Figure 2.5 UV-Vis spectra for the carbon monoxide (—), Deoxy (---) and Metaquo (....) HbI, together with their distinctive Soret and Q bands.**

coefficient at the  $\lambda_{\max}$ . The corresponding absorptivity coefficient ( $\epsilon$ ) of the hemoglobin state was determined previously (27). Table 2.1 shows the  $\lambda_{\max}$  of each complexes and the corresponding  $\epsilon$ . For example, using the spectra of met-aquo HbI in Figure 2.5, the  $\lambda_{\max} = 407$  nm, and the corresponding  $\epsilon = 178 \text{ mM}^{-1}\text{cm}^{-1}$ . The concentration is obtained using:

$$c = A/b \epsilon \quad \text{Equation 2}$$

**Table 2.1 The spectral properties:  $\lambda_{\max}$ , and the corresponding absorptivity coefficients ( $\epsilon$ ), for HbI ferrous and ferric complexes (27)**

Complex	$\lambda_{\max}$ (Soret) (nm)	$\epsilon$ ( $\text{mM}^{-1}\text{cm}^{-1}$ )	$\lambda_{\max}$ (Q) (nm)	$\epsilon$ ( $\text{mM}^{-1}\text{cm}^{-1}$ )
<i>Deoxy - HbI</i> ( $\text{Fe}^{\text{II}}$ )	433	119	557	12.2
<i>Metaquo - HbI</i> ( $\text{Fe}^{\text{III}}$ )	407	178	502, 633	10.2, 4.2
<i>Carbon monoxy -HbI</i> ( $\text{Fe}^{\text{II}}$ )	421	189	539, 570	13.2, 12.2

## 2.7 Fourier Transformed Infrared (FT-IR) Studies of HbI mutants

### 2.7.1 Deoxy and Carbon monoxide Heme complexes Preparations

Two different complexes were prepared for the vibrational spectroscopy studies of the carbon monoxide and the deoxy forms of HbI mutants. The deoxy derivatives for the HbI mutant's samples were prepared by adding a solution of sodium dithionite ( $\text{Na}_2\text{S}_2\text{O}_4$ ). This solution was prepared with a concentration of 200 mM  $\text{Na}_2\text{S}_2\text{O}_4$  (Sigma) and 100 mM potassium bisphosphate (Fisher). First,  $\sim 60 \mu\text{L}$  of the hemoglobin wastransferred to a

“small mini-tube” and tightly sealed with a rubber septum. The sample was purged with gaseous nitrogen (99.0%, Linde Gas) for 10 minutes in order to remove any oxygen present from it. Approximately 2-3  $\mu\text{L}$  of the sodium dithionite solution was added with a microsyringe to the sample. A UV-Vis spectrum was obtained to verify the formation of the deoxy derivative. Figure 2.5 presents the UV-Vis spectra of the deoxy complex, which showed the characteristic Soret band at 433 nm and Q band at 557 nm. The carbon monoxide derivatives for rHbI and the mutants were prepared using  $\text{Na}_2\text{S}_2\text{O}_4$  as a reducing agent, anaerobic conditions and gaseous carbon monoxide, (99.0%, Linde Gas). Then, the sample was exposed to a CO atmosphere for  $\sim 10$  minutes. The formation of the CO complexes was verified by their UV-vis spectra. Figure 2.5 shows an example of the carbon monoxide derivative, which showed the Soret band at 420 nm and Q bands at 539 and 570 nm.

### 2.7.2 FT-IR Measurements

FT-IR spectra of the carbon monoxide derivatives HbI mutants from *Lucina pectinata* were obtained using an Excalibur FTS 300 FTIR spectrophotometer (BioRad) equipped with a cryogenic mercury cadmium telluride detector cooled with liquid nitrogen. The spectrophotometer was continuously purged with dried air before each data acquisition, in order to minimize atmospheric carbon dioxide and water vapor contributions. The samples (50  $\mu\text{L}$  with a concentration 4-6 mM in heme) were placed in barium fluoride ( $\text{BaF}_2$ ) windows with path length of 0.05 mm, and their spectra were taken from  $500\text{ cm}^{-1}$  to  $4000\text{ cm}^{-1}$ . Data acquisition was carried out using commercial Bio-Rad Merlin<sup>®</sup> application software. The spectra presented here were subtracted from the deoxy derivative of the HbI

mutants and are the sum of 500 scans with a  $4\text{ cm}^{-1}$  spectral resolution. Each spectrum was baseline corrected and peaks were resolved using deconvolution protocols in the software GRAMS AI<sup>®</sup>. To determine the percent of intensity or population for each of the conformers, we used the following equation:

$$A_i / A_{\text{total}} (100\%) \quad \text{Equation 3}$$

where the  $A_i$  is the area under an individual deconvoluted peak, and  $A_{\text{total}}$  is the sum of all areas of the deconvoluted peaks.

## 2.8 Kinetics studies of HbI mutants

The kinetics experiments were performed in 100 mM succinic acid (Fisher) and 100 mM  $\text{KH}_2\text{PO}_4$  (Fisher) buffer at pH 7 using a UV-Vis Scanning Spectrophotometer SHIMADZU (UV-2101 PC Double Beam) equipped with the UV-Probe software.

### 2.8.1 Sample preparation and kinetics measurements

Approximately 300  $\mu\text{L}$  of a sample was added to a quartz cuvette and sealed with a septum. Then, it was degassed and purged with  $\text{N}_2$ , and reduced using the solution of  $\text{Na}_2\text{S}_2\text{O}_4$ , as described previously. To determine the concentration of the sample and verify the formation of the deoxy-HbI complex, a UV-Vis spectrum was taken as the spectrum presented in Figure 2.5. To prepare the HbI-CO mutant solution of 1 mM CO (according to the solubility of CO in water (28)), we purged the deoxy complex with gaseous CO (99.0%, Linde Gas). Since the measurement was carried out using replacement reaction with a saturated solution of NO. A NO solution was prepared degassing and saturating  $\sim 15\text{ mL}$  of buffer with NO gas (99%, Sigma Aldrich) at 1 atm to produce a stock solution of 2 mM of

NO in solution (28). The solution containing the HbI mutant-CO was rapidly mixed with the buffer equilibrated with NO in a quartz cuvette. To determine the volume of the HbI-CO to be added for the reaction we used the dilution equation (Equation 4).

$$C_1V_1 = C_2V_2 \quad \text{Equation 4}$$

where the  $C_1$  is the concentration determined by the Beer-Lambert Law previously,  $V_1$  is the volume of the HbI mutant CO derivative to be added,  $C_2$  is the desired concentration of the HbI-CO (12  $\mu\text{M}$ ) and  $V_2$  is the final volume of solution (1.5 mL). Rearranging Equation 4 we obtained Equation 4, which we determined the volume of the HbI-CO complex to be added:

$$V_1 = C_2V_2 / C_1 \quad \text{Equation 5}$$

The reaction was followed at 420 nm under flooding conditions where it is presumed that  $[\text{NO}] \gg [\text{HbI-CO}]$ . The CO dissociation rate constant for each HbI mutants at the E11 position were determined using a non-linear least-square program, OriginPro<sup>®</sup> 7.5 software.

## 3 RESULTS

### 3.1 UV-Vis measurements of CO HbI mutant derivatives

Heme proteins can absorb visible and ultraviolet light (7,28). The UV-Vis spectrum of the heme shifts depending of the electronic configuration of the metallic center (iron) in the heme. As mentioned before, the UV-Vis spectrum for heme proteins presents two classical types of bands called the Soret and the Q bands. Through time, the UV-Vis spectrum of heme protein have been used for identify heme-ligand complexes. It is observed that depending of ligand bound or oxidation state of the Fe, the position of the bands change. In this work, the UV-Vis spectrum was used to monitor the formation of the deoxy and carbon monoxy complexes with each HbI mutants, before FT-IR and kinetics measurements. Figures 3.1 present the UV-Vis spectra for rHbI, HbI PheE11Val, HbI PheE11Gln, and HbI PheE11Tyr with CO. Each spectrum shows the Soret at 421 nm and Q-bands at 539 and 570 nm characteristic of the complex in concordance to the previous studies (24). This similarity confirmed the formation of the CO derivative.

### 3.2 FT-IR measurements of CO derivatives

FT-IR spectroscopic studies are a useful tool for the characterization of protein secondary structure and the identification of components involved in ligand binding, among others (9). This part of the chapter presents the acquired FT-IR data for the ferrous carbon monoxide derivatives (HbI-CO). The importance and the role of the E11 position was studied by mutating the Phe with three amino acids: Val, Gln and Tyr.

#### 3.2.1 FT-IR measurements of CO derivatives with HbI mutants at E11 position

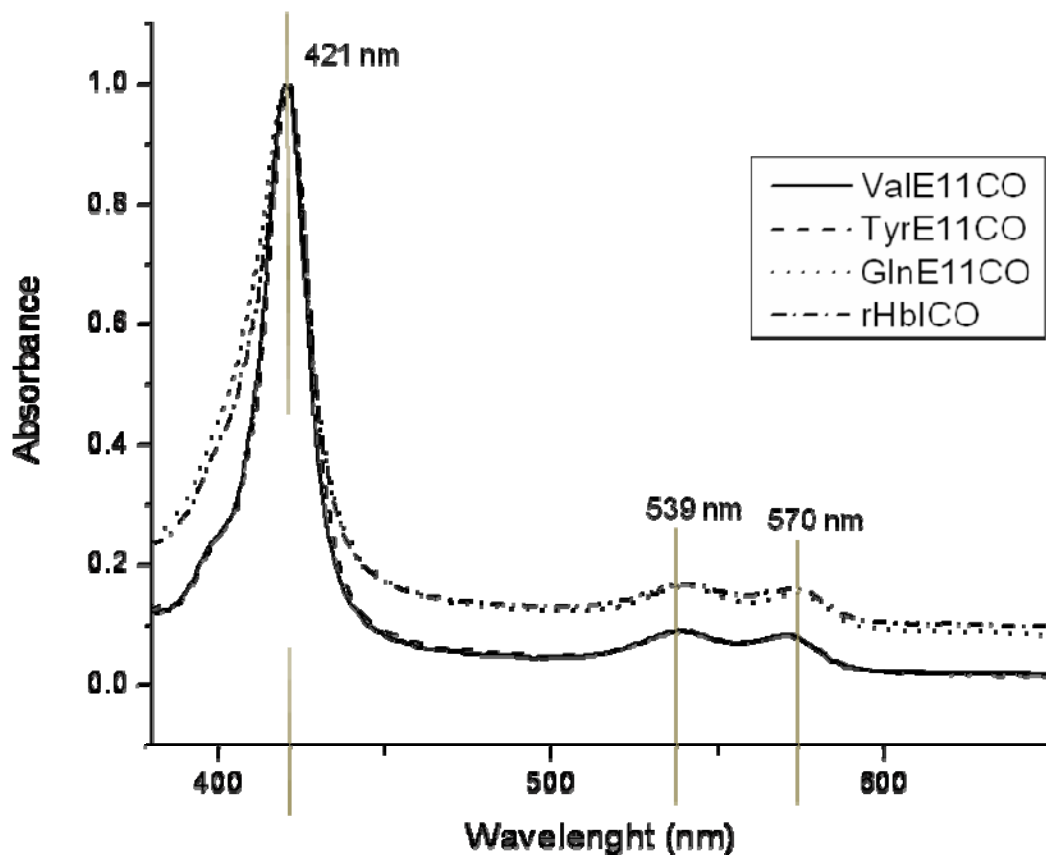


**Figure 3.1 UV-Spectra of the HbI mutants at the E11 position with CO as ligand. This spectra shows the Soret band at 421 nm and the Q bands at 539 and 570 nm.**

According to several studies of the binding of CO to heme proteins, it has been found that CO shows several stretching frequencies ( $\nu_{\text{CO}}$ ). As mentioned before, in mammalian myoglobin are observed three  $\nu_{\text{CO}}$ , corresponding to different conformers, in their FT-IR spectrum. The three  $\nu_{\text{CO}}$  are positioned at:  $1965\text{ cm}^{-1}$ ,  $1945\text{ cm}^{-1}$  and  $1932\text{ cm}^{-1}$  assigned to  $A_0$ ,  $A_{1,2}$ , and  $A_3$  conformers, respectively. Each conformer has been assigned to distinct conformations produce by non-bonding and bonding interactions of the bound CO with surrounding amino acids in the heme pocket, especially with the distal E7 residue as mentioned previously. Normally, in FT-IR studies of heme-proteins, the CO stretching bands are observed using the deoxy-HbI derivative as a background. The deoxy-HbI spectrum does not show any bands in the vibrational CO region ( $1900\text{ to }2000\text{ cm}^{-1}$ ) of the IR spectrum. Then using spectrum subtraction, a better signal to noise can be obtained for the HbI-CO derivatives. Any signal resulting from the HbI-CO interactions will be improved and enhance from the background signal as we did with our measurements.

Each of these mutations produces a FTIR spectrum at different vibrational frequencies and relative intensities. Figures 3.2-3.5 show the deconvoluted FTIR spectrum obtained by the best residual plot of the CO stretching bands and their relative intensities for the rHbI as well for the HbI mutants at the E11 position. For example, Figure 3.2, shows the FTIR spectrum for the rHbI which yielded one major  $\nu_{\text{CO}}$  band at  $1936\text{ cm}^{-1}$ , a minor one at  $1960\text{ cm}^{-1}$ , and a very small band at  $1950\text{ cm}^{-1}$  with 62%, 31% and 7% of relative intensities, respectively. These CO stretching bands are the same observed by Navarro *et al.*, (22) with the wild-type HbI. Each band was assigned as a different conformational state of the amino

acids in the heme pocket. The band at  $1940\text{ cm}^{-1}$  was designated to a close conformation ( $A_3$ ), in which a synergetic interaction occurs with the amino acids E7, B10 and E11 residues in HbI with the CO bound. A close conformation ( $A_{1,2}$ ) was assigned to the band at  $1950\text{ cm}^{-1}$ , where the GlnE7 is having a hydrogen bond interaction with the bounded CO. Finally, the band at  $1960\text{ cm}^{-1}$  was ascribed to open conformation ( $A_o$ ) where any type of interactions are observed with the ligand. Figure 3.3, shows the FTIR spectrum for the HbI PheE11Val. The replacement of the Phe for a small and aliphatic amino acid (Val) generates only two deconvoluted  $\nu_{CO}$ : a mayor peak at  $1942\text{ cm}^{-1}$  (76%) and other at  $1955\text{ cm}^{-1}$  (24%). In comparison with the rHbI, the intensities of these peaks increased by 14% and 17% respectively, and the frequencies shifted to higher energies. Also, it is clear that the peak at  $1960\text{ cm}^{-1}$  disappeared. The wild-type sperm whale myoglobin (SW-Mb) which possesses a ValE11, displayed a similar FT-IR spectrum as HbI PheE11Val with two  $\nu_{CO}$  at  $1945$  and  $1932\text{ cm}^{-1}$  (11). Substitution of the PheE11 by an aromatic and polar residue such as Tyr, produced a FT-IR spectrum that can be deconvoluted on three different peaks: a mayor at  $1941\text{ cm}^{-1}$  (63%), a minor one at  $1962\text{ cm}^{-1}$  (34%) and a small peak at  $1954\text{ cm}^{-1}$  (3%) as shown in Figure 3.4. The peaks shifted to higher frequencies in comparison with those of rHbI. The percent of intensity increased by 1% and 3% in the  $A_3$  and  $A_o$  conformers, respectively. However, it is observed that the  $A_{1,2}$  conformer decreased by 4%. Furthermore, Figure 3.5 shows the FT-IR spectrum for HbI PheE11Gln, where the PheE11 is replaced by this polar amino acid, Gln. The FT-IR spectrum generated is similar to the rHbI showing a well-defined major band at  $1939\text{ cm}^{-1}$  (64%), a minor one at  $1960\text{ cm}^{-1}$  (22%) and a small

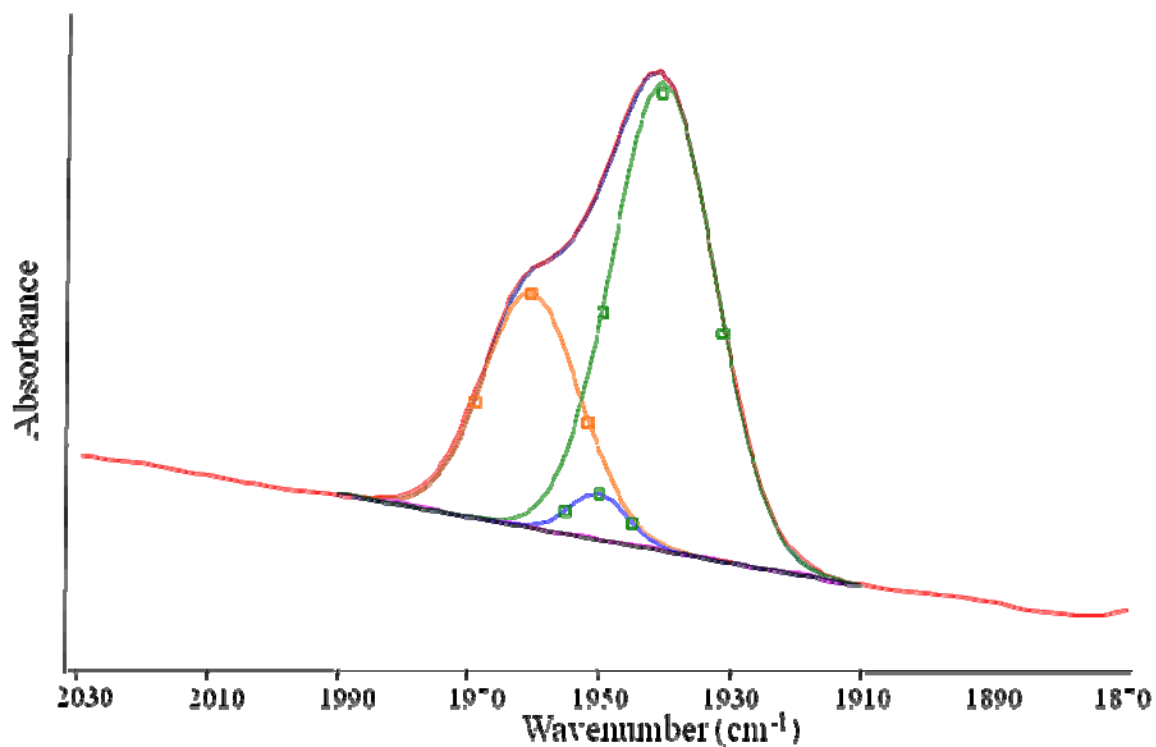


**Figure 3.2** The FT-IR spectrum of the CO stretching bands obtained for rHbl. In the spectrum, it is shown the experimental data (red), the best data fit (navy blue), and the residual (pink). The obtained deconvoluted CO stretching bands are shown here: in orange for the A<sub>0</sub> conformer (1960 cm<sup>-1</sup>), light blue for the A<sub>1,2</sub> conformer (1950 cm<sup>-1</sup>), and the one green line for A<sub>3</sub> (1936 cm<sup>-1</sup>).

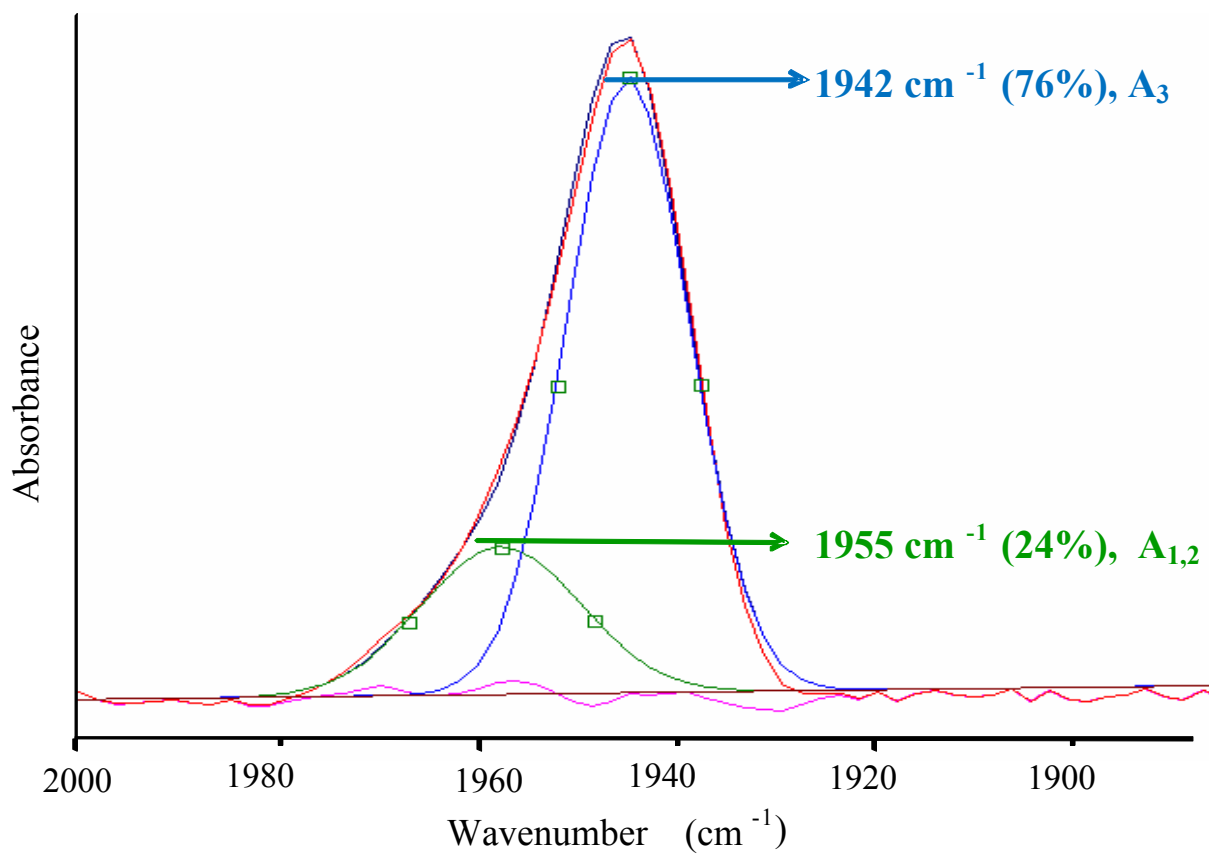


**Figure 3.3** The FT-IR spectrum of the CO stretching bands obtained for the HbI PheE11Val. The spectrum, it is shown the experimental data (red), the best data fit (navy blue), the residual (pink), and the obtained deconvoluted CO stretching bands (green and light blue).

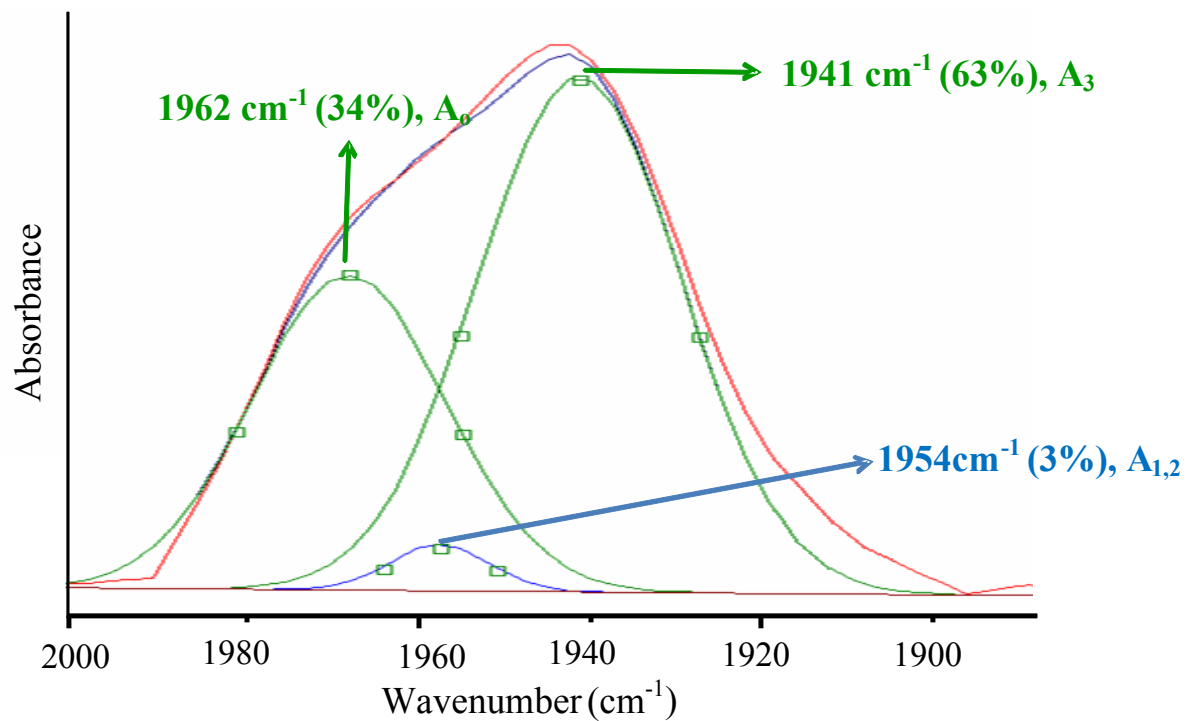


**Figure 3.4** The FT-IR spectrum of the CO stretching bands obtained for the HbI PheE11Tyr. In the spectrum, it is shown the experimental data (red), the best data fit (navy blue), the residual (pink), and the obtained deconvoluted CO stretching bands (green and light blue).

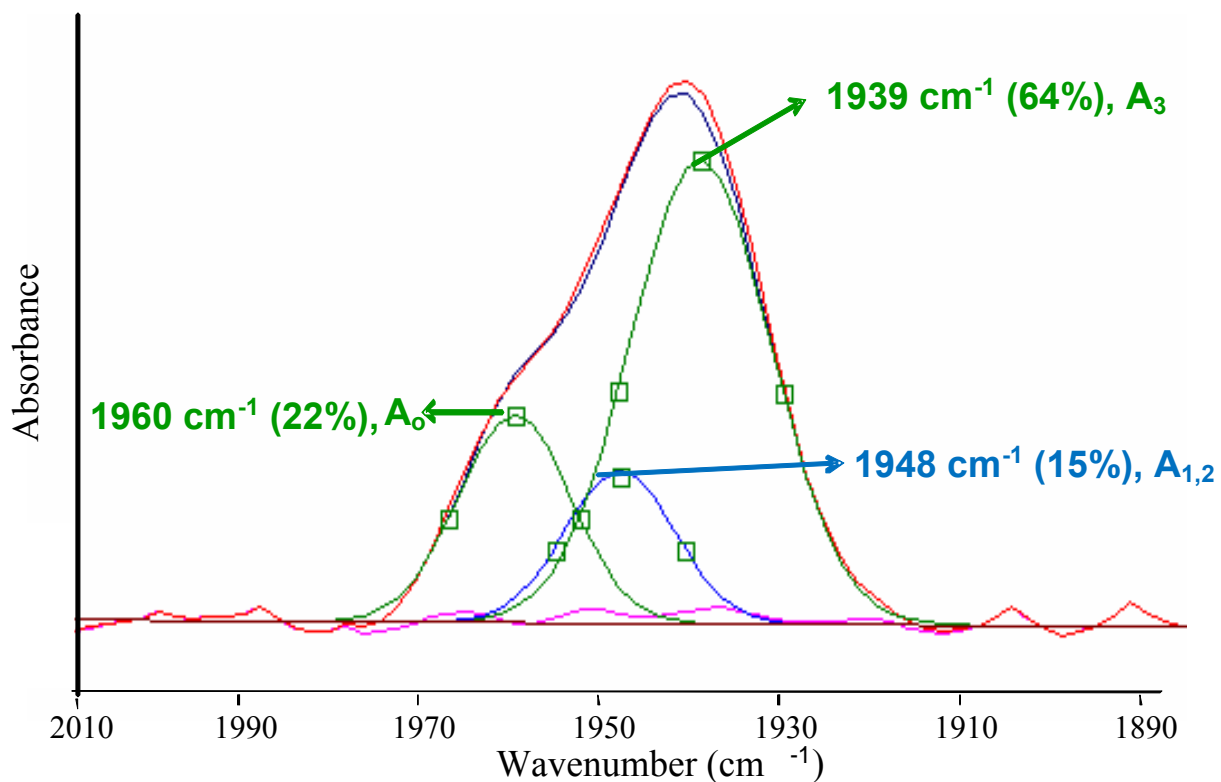


**Figure 3.5** The FT-IR spectrum of the CO stretching bands obtained for the HbI PheE11Gln. In the spectrum, it is shown the experimental data (red), the best data fit (navy blue), the residual (pink), and the obtained deconvoluted CO stretching bands (green and light blue).

band at 1948 cm<sup>-1</sup> (15%). No considerable differences between the vibrational frequencies are observed, when the two are compared. The percent of differences compared to the rHbI varies from 2% – 9% in relative intensities. These results suggest that the Phe at the E11 position in HbI may contribute in the positioning of the other amino acids in such way that allows the stabilization of the bound CO in heme environment of HbI due to the increase in population of the closed conformer (A<sub>3</sub>).

### 3.3 Kinetics rate constant for the dissociation of CO

For the determination of CO dissociation rate constant values, we referred to the following reaction:



The reaction was studied under flooding conditions where the NO concentration was at least 10<sup>2</sup> times the concentration of HbI-CO (~12μM). Figure 3.6 to 3.9 show the plot of absorbance at 420 nm vs. time for the reaction of the rHbI and the E11 HbI mutants. The kinetics trace for this reaction presents a decrease in absorbance (420 nm) with time. The data was modeled using an exponential decay fit provided by OriginPro<sup>®</sup> 7.5, using the following equation:

$$y = A_1 e^{(-x/t_1)} + y_o \quad \text{Equation 6}$$

where y is the dependent variable, y<sub>o</sub> is the y offset, A<sub>1</sub> is the amplitude, x is the independent variable and t<sub>1</sub> is the decay constant. These variables are proved to be mathematically equivalent (see Appendix 1) to the following equation:

$$A_t = (A_o - A_{inf}) e^{-kt} + A_{inf} \quad \text{Equation 7}$$

where  $(A_0 - A_{inf}) = A_1$ ,  $A_{inf} = y_0$ ,  $A_t = y$ ,  $t = x$ , and  $k = (t_1)^{-1}$ . In this example  $(A_0 - A_{inf}) = 0.0644$ ,  $A_{inf} = 0.1973$ , and  $k_{obs} = 0.007 \text{ s}^{-1}$ .

Table 3.1 presents the dissociation  $k_{obs}$  values for the reactions corresponding to all the HbI mutants at the E11 position studied. It is observed that mutation at the E11 position has only a subtle effect on the rate constants. Neither of the HbI PheE11Tyr and HbI PheE11Val presents a significant increment in the dissociation  $k_{obs}$ , compared with the rHbI. However, the dissociation  $k_{obs}$  values for HbI PheE11Gln increased ~2-fold compared to the rHbI. It has been found that the dissociation rate constants for several mutants at the E11 position in SW-Mb and leghemoglobin do not present significant changes as it is observed here in HbI mutants (28).

**Table 3.1 The CO dissociation observed rate constants for the rHbI and the HbI mutants at the E11 position**

<b>Protein</b>	<b><math>k_{obs} \text{ CO (s}^{-1}\text{)}</math></b>
rHbI	$0.0080 \pm 0.0005$
HbI PheE11Val	$0.0104 \pm 0.0002$
HbI PheE11Gln	$0.0050 \pm 0.0004$
HbI PheE11Tyr	$0.0093 \pm 0.0001$

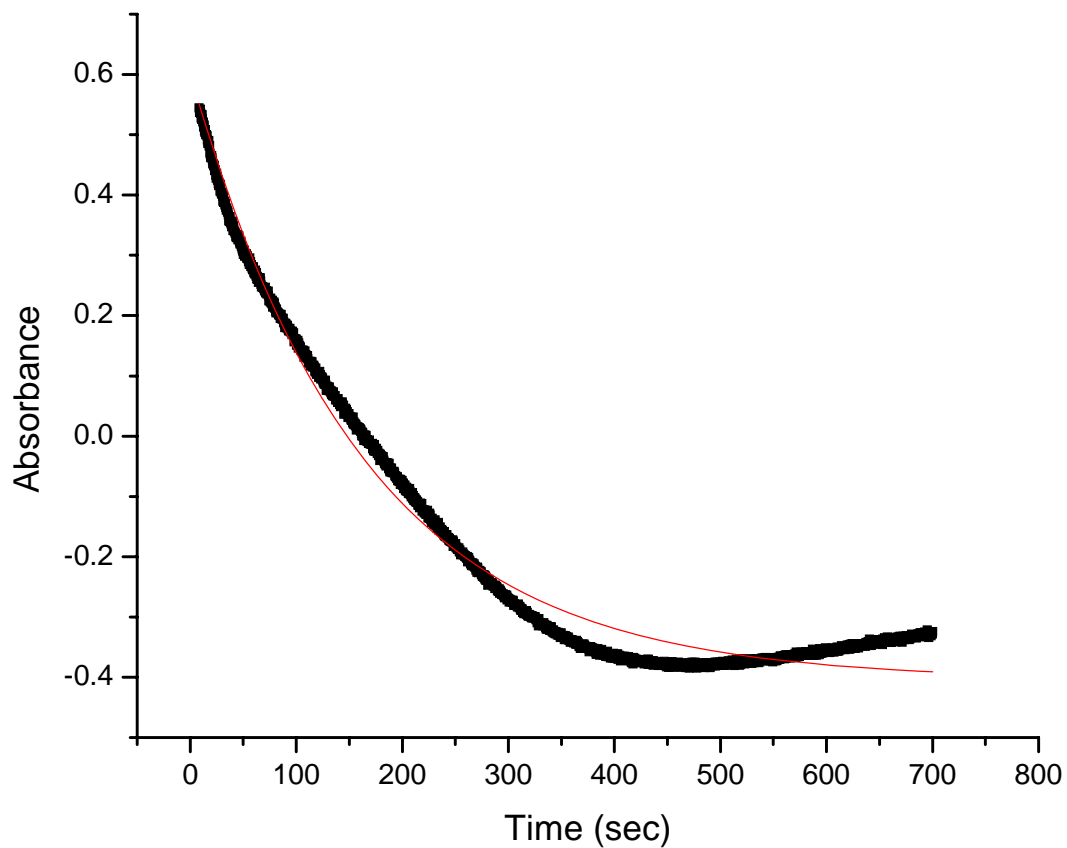


**Figure 3.6** Plot of absorbance at 420 nm vs. time for the replacement reaction of CO in rHbI, under flooding conditions where  $[\text{NO}] \gg [\text{HbI-CO}]$ . The continuous red shows the best behavior of the experimental data which is described by the following mathematical equation,  $y = 0.6264 e^{-0.008x} - 0.7056$ .

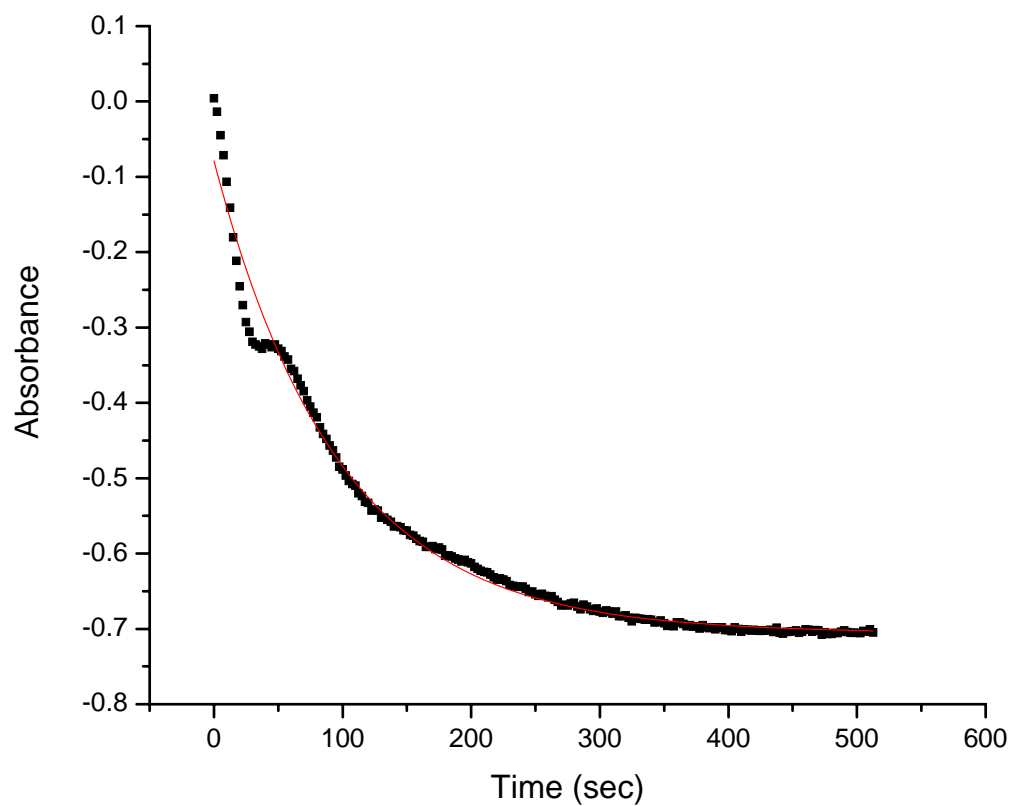


**Figure 3.7** Plot of absorbance at 420 nm vs. time for the replacement reaction of CO in HbI PheE11Val, under flooding conditions where  $[NO] \gg [HbI-CO]$ . The continuous red shows the best behavior of the experimental data which is described by the following mathematical equation,  $y = 1.0060 e^{-0.010x} - 0.4044$ .

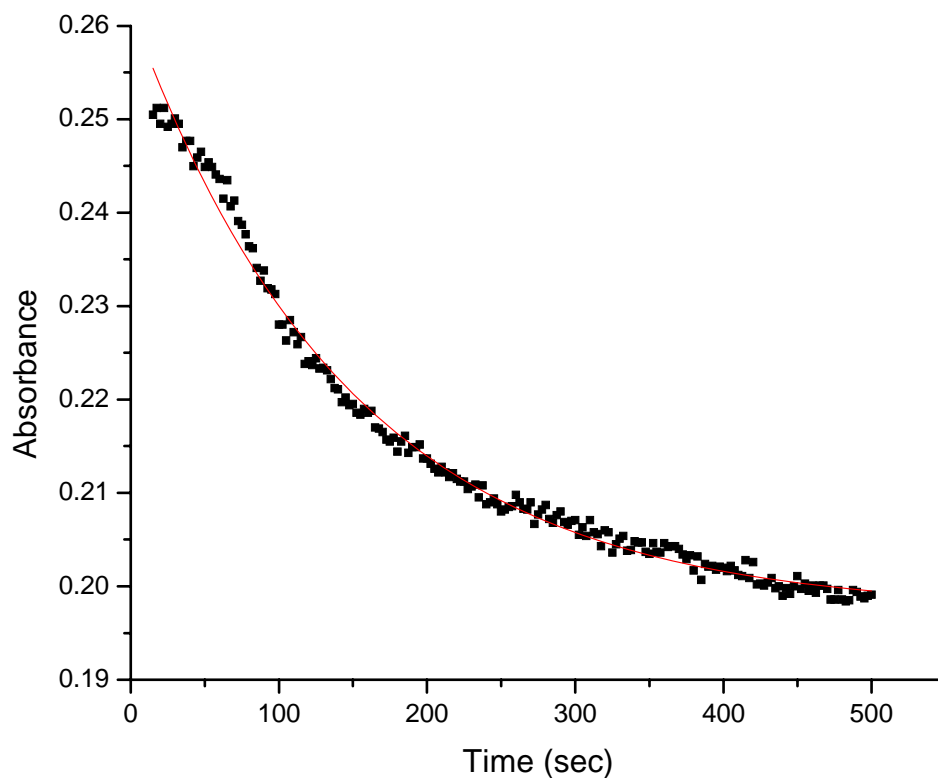


**Figure 3.8** Plot of absorbance at 420 nm vs. time for the replacement reaction of CO in HbI PheE11Gln, under flooding conditions where  $[\text{NO}] \gg [\text{HbI-CO}]$ . The continuous red shows the best behavior of the experimental data which is described by the following mathematical equation,  $y = 0.4038 e^{-0.005x} - 0.1428$ .

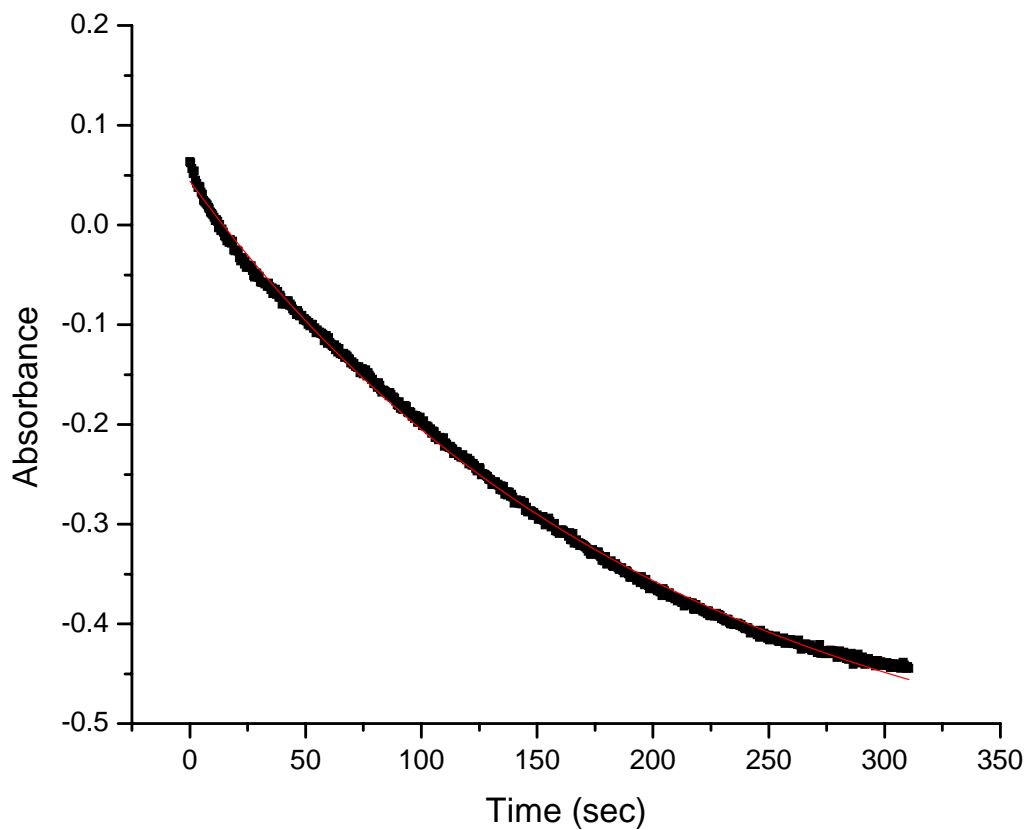


**Figure 3.9** Plot of absorbance at 420 nm vs. time for the replacement reaction of CO in HbI PheE11Tyr, under flooding conditions where  $[NO] \gg [HbI-CO]$ . The continuous red shows the best behavior of the experimental data which is described by the following mathematical equation,  $y = 0.3179 e^{-0.009x} - 0.5919$ .

## 4 DISCUSSION

### 4.1. Interpretation of the CO vibrational frequencies in HbI mutants at the E11 position

Carbon monoxide has been used widely as a vibrational probe of heme proteins to examine the heme distal site (10). In ferrous mammalian myoglobin presents various  $\nu_{\text{CO}}$ , and they have been characterized (11) and assigned to different heme conformations. Three different structural states have been assigned: an open conformation ( $A_0$ ) with  $\nu_{\text{CO}}$  at  $\sim 1965 \text{ cm}^{-1}$ , and a weak-closed conformation ( $A_{1,2}$ ) with a  $\nu_{\text{CO}}$  at  $\sim 1945 \text{ cm}^{-1}$ , and closed conformation ( $A_3$ ) with a  $\nu_{\text{CO}} \sim 1932 \text{ cm}^{-1}$ .

Considering the existence of these structural states, the CO stretching bands observed in wild-type HbI (wt-HbI) from *Lucina pectinata* have been assigned to different residue-ligand interactions. The conformer centered at  $1960 \text{ cm}^{-1}$  ( $A_0$ ) indicates the absence of strong polar interaction between the distal pocket residues and the bound CO. The  $A_3$  conformer with a  $\nu_{\text{CO}}$  value of  $1936 \text{ cm}^{-1}$  has been attributed to a closed structure in which a synergetic effect between the GlnE7, PheB10 and the PheE11 produced a strong positive electrostatic environment near the CO bound. It has been suggested that in this conformer the GlnE7 interacts through a hydrogen bond interaction with the CO, as well as multipole interactions of the Phe residues (at the B10 and E11 position) with the ligand. The  $A_{1,2}$  conformer (at  $\sim 1950 \text{ cm}^{-1}$ ) is ascribed to a closed structure produced by the GlnE7, which is having hydrogen bond interaction with the CO. (22,23) Table 4.1 summarizes the CO stretching frequencies for the rHbI, the HbI mutants (HbI PheE11Val, HbI PheE11Gln, and HbI PheE11Tyr), and SW-Mb. The IR spectrum for rHbI displayed the three  $\nu_{\text{CO}}$ , same as in the

**Table 4.1 CO stretching frequencies for recombinant, HbI mutants at the E11 position form *Lucina pectinata* and SW-Mb**

<b>Protein</b>	<b>A<sub>0</sub> (%) cm<sup>-1</sup></b>	<b>A<sub>1,2</sub> (%) cm<sup>-1</sup></b>	<b>A<sub>3</sub> (%) cm<sup>-1</sup></b>
wt-HbI	1960 (30)	1950 (9)	1936 (61)
rHbI	1960 (31)	1950 (7)	1936 (62)
HbI PheE11Val		1955 (24)	1942 (76)
HbI PheE11Gln	1960 (22)	1948 (15)	1939 (64)
HbI PheE11Tyr	1962 (34)	1954 (3)	1941(63)
SW-Mb <sup>a</sup>		1945 (70)	1932 (30)
SW-Mb Double mutant <sup>a</sup>		1950 (35)	1937 (65)

<sup>a</sup>Data from reference 11

wt-HbI. This implies that both heme-proteins are structurally analogous. Replacement of PheE11 by a polar amino acid such as Gln produced a similar spectrum as in rHbI. However, a decrease of 9% is observed for the population of the A<sub>0</sub> conformer, while an increase of 6% is detected in population of the A<sub>1,2</sub> conformer compared to rHbI. This implies that in some way the distal pocket residues are producing a positive electrostatic field around the CO bound. Hence, we can suggest that an increase in positive electrostatic field is produced by hydrogen bonding and/or multipole interactions developed, principally, by the GlnE7 and PheB10. The distal site of truncated hemoglobins (trHb), particularly from the green algae *Chlamydomonas eugametos* (trHbC) and *Synechocystis sp. PCC 6803* (trHbS), contain a Gln, Tyr and Gln at the E7, B10 and E11 positions, respectively. In these trHbs, GlnE11 has polar

interactions with the amino acids nearby and the bound ligand. This interaction allows the ligand stabilization by orienting the B10 residue at a particular position in the distal site. Furthermore, it has been found that mutations may cause the E-helix to move in such way that permits the E7 and E11 amino acids get closer to the heme iron (2). Similar to trHbs, the presence of a polar residue at the E11 position (HbI PheE11Gln) suggests a possible structural displacement, which allows for a few degrees of movement of other residues (particularly B10). This movement could promote the multipole electrostatic interaction around the bound CO increasing the population of the close conformers. Also, this displacement can be accomplished with a movement of the E-helix in order to enhance the interaction between the GlnE7 and the bound ligand. Moreover, recent molecular dynamics simulation studies have demonstrated that mutation in the E11 position produced a structural displacement that allows the PheB10 get closer to the heme iron, as it is shown in Figure 4.1 (28). This is further supported by the FT-IR results of the HbI PheE11Val, which caused the disappearance of the  $A_0$  conformer and the increase of 14% and 17% in the population of the  $A_3$  and  $A_{1,2}$  conformers, respectively. This suggests that a positive electric field or hydrogen bond interactions are produced near the bound ligand. As mentioned before, this positive electric field is possibly caused by the GlnE7 and the PheB10 residues due to structural changes induced by the substitution of PheE11, which allows both residues to move toward the ligand to make a closer structure. In sperm whale myoglobin (SW-Mb), the position E11 is occupied by a valine (Val). The IR spectrum showed the presence of just two bands: a major at  $1945\text{ cm}^{-1}$  ( $A_{1,2}$  conformer), and a minor at  $1932\text{ cm}^{-1}$  ( $A_3$  conformer) (11) as in HbI

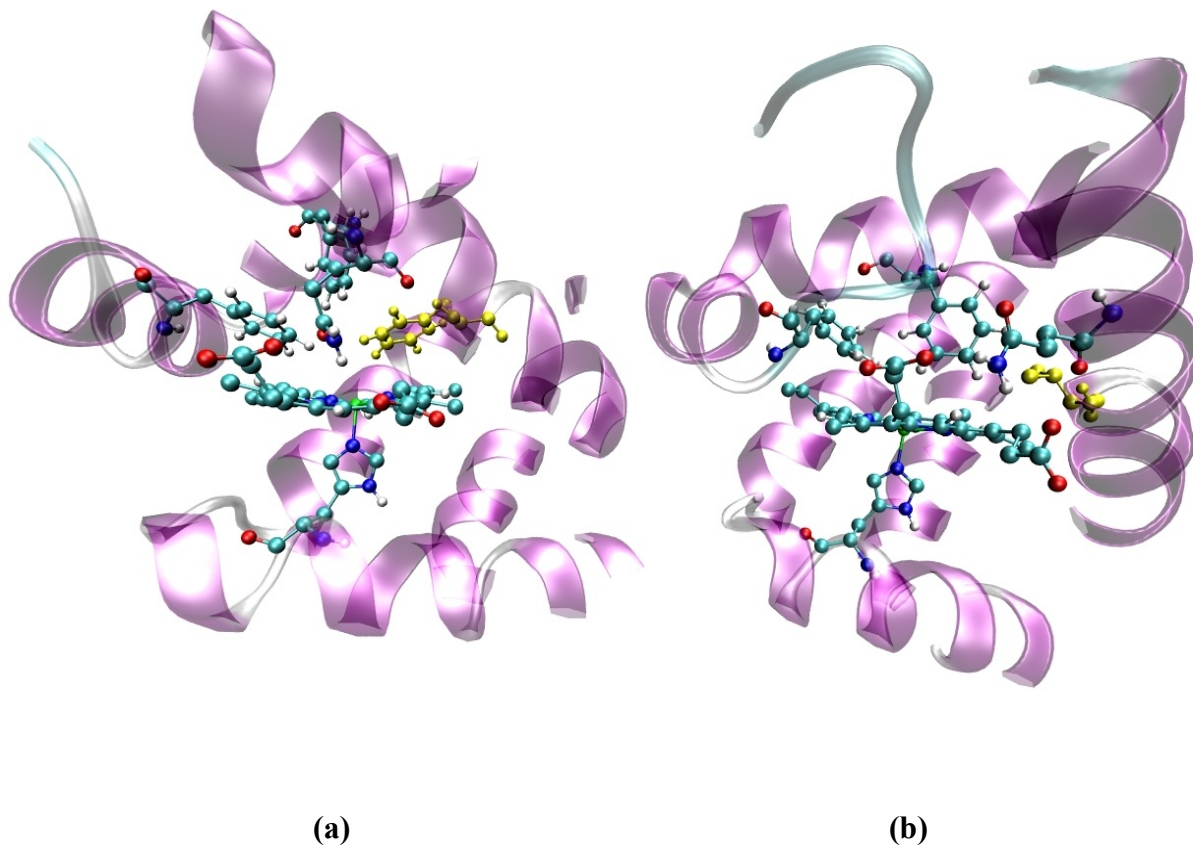


**Figure 4.1** Molecular dynamic scheme of the HbI structure of the (a) wt-HbI, and (b) HbI PheE11Val. The heme group and the residues are show in ball-sticks representation, while the different helix are shown as ribbons. The residue in yellow color is Phe in (a) and Val in (b).

PheE11Val. FT-IR studies with a SW-Mb double mutant, which bears Phe, Gln and Val in the B10, E7, and E11 position respectively, displayed the same FT-IR spectrum as the SW-Mb, and HbI PheE11Val. These results suggest that the side chain of the residue at the E11 position in both Mb and HbI may play a similar role. In this respect, mutations at this position (E11) in SW-Mb have been found to influence the MbCO IR spectra significantly (11). The IR changes were attributed to the fact that ValE11 in SW-Mb is very close to the heme iron atom. The observed short distance allows the ValE11 to sterically hinder the binding of ligand. Also, it has been established from these and other studies that ValE11 is important for maintaining the appropriate distal pocket volume for ligand binding (3, 28). Also, Thus, these results strongly suggest that the PheE11 is a structural “controller”, in terms of maintaining the HbI distal heme site volume as in Mb. Moreover, these findings along with the results presented here, suggest that in HbI, the E11 residue could be influencing ligand binding in the same way. Furthermore, these results are supported by analyzing the HbI PheE11Tyr. This mutant displayed an IR spectrum similar to rHbI with the overall band showing a broader spectrum. These broaden in the IR spectrum have been related to the existence of small populations of intermediate conformers which implies structural changes in the distal heme pocket (11, 30). In such way, these structural changes decrease the degree of positive electric field or decrease the degree of hydrogen bond interactions in the HbI PheE11Tyr. The  $\nu_{CO}$  shifted to higher wavenumbers, which confirms the weakening of the electrostatic interactions. According to Pietri, *et al.*, (23) when PheB10 is changed for a Tyr, the FTIR spectrum produces just two bands: a major band at  $\sim 1927$

cm<sup>-1</sup> (75%) and a minor band at ~ 1967 cm<sup>-1</sup> (25%). The explanation for these finding was that PheB10 contributes positively to the A<sub>3</sub> conformer stabilizing the CO in a closed configuration by increasing the overall positive electrostatic field in the distal heme pocket of HbI. Nevertheless, the HbI PheE11Tyr displayed three CO stretching bands, in contrast to the HbI PheB10Tyr. This comparison supported the idea that the PheE11 contributes to the formation of the A<sub>3</sub> conformers due to the structural stabilization in HbI distal heme environment, which at the same time promotes polar interactions with the bound ligand.

#### **4.2. Implications of the FT-IR results in ligand binding and stabilization**

The analysis of the FT-IR frequencies, kinetics rate constant values of CO dissociation and O<sub>2</sub> support the idea that PheE11 plays an important role in ligand-binding and structural stabilization within wt-HbI. Table 4.2 presents kinetics rate constants of CO and O<sub>2</sub> for rHbI and the HbI mutants studied here. In the HbI mutants, the dissociation  $k_{obs}$ , for CO showed small differences between each other. Neither of the HbI mutants presents a significant increase or decrease in their dissociation  $k_{obs}$  values. This suggests that mutations at this position provoke similar structural changes, which prevent a fast dissociation of the CO. Moreover, the association rate constants for CO ( $k_{onCO}$ ) in two HbI mutants, PheE11Val and PheE11Tyr (0.010 sec<sup>-1</sup> and 0.009 sec<sup>-1</sup>, respectively), are practically the same between each other, but increase 30-fold when compared with the rHbI ( $k_{onCO} = 7.2 \mu\text{M}^{-1}\text{s}^{-1}$ ). The same behavior is observed with the association rate constant of oxygen ( $k_{onO_2}$ ). The  $k_{onO_2}$  observed for the HbI PheE11Val and HbI PheE11Tyr are 120 and 110  $\mu\text{M}^{-1}\text{s}^{-1}$ , respectively. As it can be observed, the  $k_{onO_2}$  value is practically the same between the HbI mutants and the

**Table 4.2 Kinetic dissociation and association rate constants of CO and O<sub>2</sub> for the rHbI and the HbI mutants at the E11 position**

<b>Protein</b>	<b>Amino acids E7 B10 E11</b>	<b>k<sub>obs</sub> CO s<sup>-1</sup></b>	<b>k<sub>on</sub> CO<sup>b</sup> μM<sup>-1</sup>s<sup>-1</sup></b>	<b>k<sub>on</sub> O<sub>2</sub><sup>b</sup> μM<sup>-1</sup>s<sup>-1</sup></b>	<b>k<sub>off</sub> O<sub>2</sub><sup>b</sup> s<sup>-1</sup></b>
rHbI	Gln Phe <i>Phe</i>	0.008	7.2	190	140
HbI PheE11Val	Gln Phe <i>Val</i>	0.010	16	120	325
HbI PheE11Gln	Gln Phe <i>Gln</i>	0.005	NA	NA	NA
HbI PheE11Tyr	Gln Phe <i>Tyr</i>	0.009	17	110	40
SW-Mb	His Leu <i>Val</i>	0.005	0.51 <sup>c</sup>	17 <sup>c</sup>	15 <sup>c</sup>

<sup>b</sup> Data unpublished by Ruth León, *et al.*, <sup>c</sup> Data from reference , NA = data not available

only difference with respect to rHbI is a reduction of ~ 2-fold in k<sub>onO<sub>2</sub></sub>. Together, these findings suggest that: (i) mutations of the E11 position, no matter size and polarity of the amino acid, produces the same conformational changes due to the similar behavior observed in the k<sub>on</sub> for O<sub>2</sub> and CO, and (ii) the increase in k<sub>onCO</sub> and the decrease of k<sub>onO<sub>2</sub></sub> is due to the chemical properties of the ligands. For example, in SW-Mb, which has a water molecule in its distal site, it has been found that the displacement of this molecule inhibits the binding of CO and O<sub>2</sub>. However, the binding of O<sub>2</sub> is improved because of its polar nature, while it inhibits in the case of CO, due to apolar nature (31). Also, it has been suggested that the O<sub>2</sub> and CO binding were limited by the ligand migration and the iron-ligand bond formation, respectively (32). On the other hand, the oxygen dissociation rate constants (k<sub>offO<sub>2</sub></sub>) for the

HbI PheE11Val and HbI PheE11Tyr are very different to each other. The  $k_{\text{offO}_2}$  values for HbI PheE11Val increases 22-fold compared with rHbI, which suggests a weakening in the hydrogen bond interactions between the nearby amino acids and the bound ligand. However, the  $k_{\text{offO}_2}$  for the HbI PheE11Tyr decreased 4-fold, compared with rHbI, which implies a strong interaction (hydrogen bonding) of the nearby residues with the oxygen bound. These analyses suggest that structural changes are occurring as mentioned before, and that the differences between the  $k_{\text{off O}_2}$  indicate the possible role of E11 in the control of ligand migration.

### **4.3 Implication and functionality of the PheE11 in the HbI**

The results presented here suggest that PheE11 does contribute to the mechanism of ligand-binding in HbI from *L. pectinata*. This contribution is made by electrostatic and steric effects due to structural changes provoked by the mutations, which may allows the positioning of the E7 and B10 residues and controlling ligand migration Moreover, this supported by studies that have demonstrated that diffusion of ligand through the protein is coupled to conformational fluctuations of residues side chains within the protein (33,34), which indicates a possible dual role of the PheE11 in HbI. In such way, the PheE11 is dictating the conformational state of HbI by influencing the position in space of the nearby residues (GlnE7 andPheB10). The presented results have demonstrated that if the PheE11 is substituted by some other amino acid, no matter the charge and size, the FT-IR spectrum presents different conformers. As shown in Figure 4.2 and according to the crystal structure of the met-aquo HbI (PDB: 1FLP), PheE11 is 3.81 Å from the PheB10. These short distance

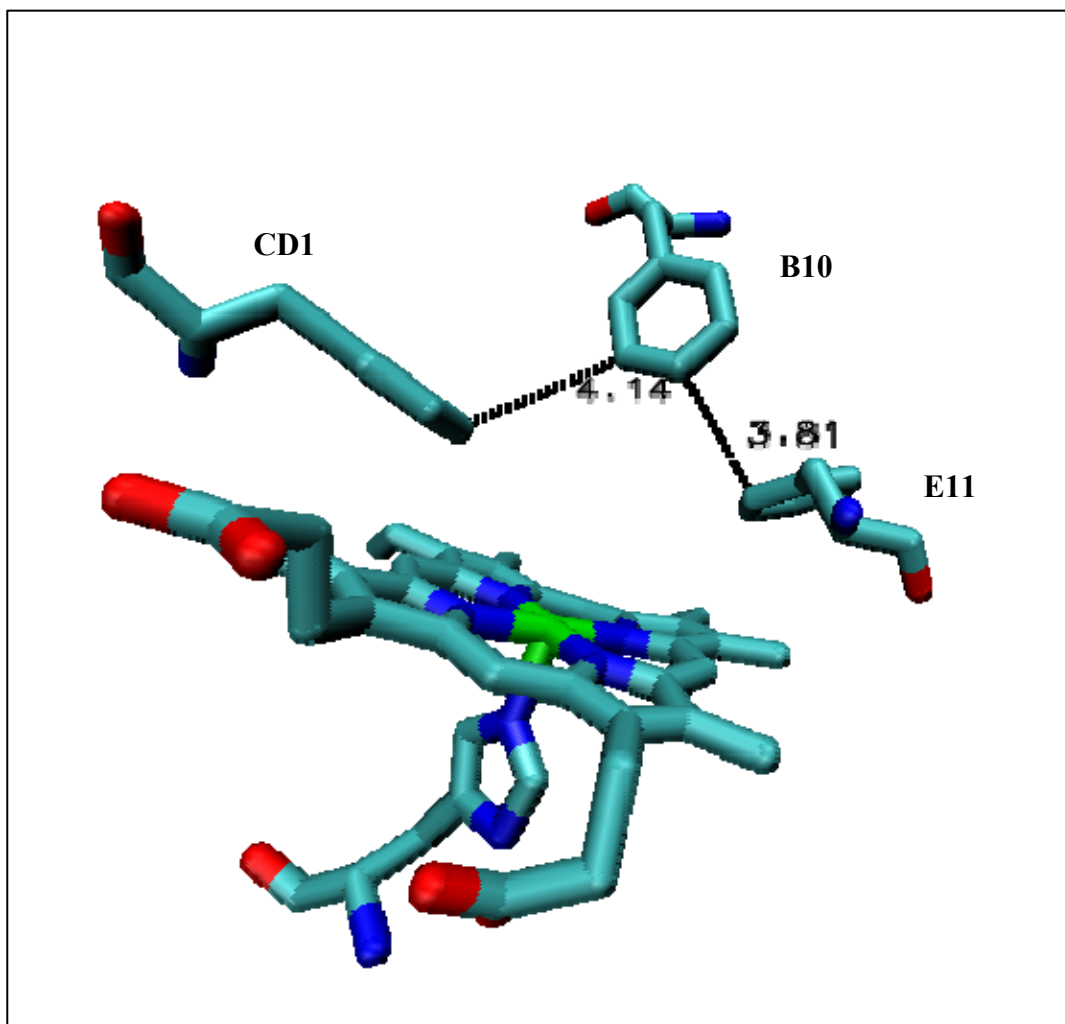


**Figure 4.2 Structure of the met-aquo wt-HbI distal pocket (PDB: FLP). The heme group and the residues are displayed as sticks representation. The Phe in the CD1, B10 and E11 position are labeled with the specific position. The dotted lines represent the distances between each amino acid. The drawings were made with VDM 1.8.5.**

between the PheE11 and PheB10 support the idea of a structural displacement in mutations because the PheE11 could cause that the PheB10 moves from its original position. Therefore, any removal of electronic density (substitution of the PheE11) could provoke a displacement of the B10 residue. These come together with the position adopted by the GlnE7, which can interact more with the ligand by hydrogen bonding for two reasons: (i) the PheE11 and GlnE7 are positioned in the same helix (E-helix), and (ii) flexibility of the GlnE7 (23). Studies of trHbs have suggested that the E-helix should rotate in order to produce the hydrogen bonding networking that stabilizes the structure of these Hbs (2,28). Moreover, recent molecular dynamics simulations confirm that HbI poses an unusual rocking freedom which allows the entrance of the ligands such as H<sub>2</sub>S, O<sub>2</sub> and CO (35), and this indicates a type of heme pocket flexibility. Also, it has been demonstrated that the GlnE7 has a degree of flexibility (23). These finding supports the hypothesis that chain rearrangements in the secondary structure are related to a structural displacement that could change the interactions between residue-residues (B10-E11). In addition, recent molecular dynamic simulations showed that mutations in the E11 position caused high degree of flexibility. According to recent studies, mutations produce conformational fluctuations and displacements which can modulate protein dynamics and ligand diffusion through the protein (36). Along with the above mentioned events, our experiments also suggest that the PheE11 plays an important role in the structural stability, which at the same time modulates the ligand internal migration. Along with this, Friedman *et al.*, (36) suggests that the residue at the E11 position in myoglobin regulates the ligand internal movement. It was showed that in ValE11Phe Mb

mutant, the ligand dissociation decreases due to a higher geminate rebinding. This increment in geminate rebinding was assigned to the benzyl side chain of the Phe, which restraint the access of the ligand to the interior of the protein. A comparable mechanism can be applied to HbI, since a 5-fold decrease in oxygen  $k_{off}$  is observed when in Mb the ValE11 is substituted by a Phe, and as well as when it is compared to the HbI PheE11Val and the wt-HbI. Therefore, we suggest that the aromatic side chain of the PheE11 is not only important in structural stabilization, but also helps to establish the ligand movement pathway in HbI. Figure 4.3 shows a squematic illustration of the possible interactions of the PheE11 in HbI, where the Phe at the E11, B10 and CD1 are showed in yellow, red and purple, respectively. The Gln at the E7 position is showed in blue, and the arrow represents the CO bound to the Fe. The dotted magenta lines represent the possible steric and hydrophobic interactions of the PheE11 with the GlnE7 and PheB10. The dash gray lines represent the electrostatic interactions of the Phe B10 and CD1 once the PheE11 positionated them in the right way. While the solid black line represent the possible hydrogen bond of the GlnE7 with the CO. These relationships between the residues in the distal pocket of HbI suggest the importance of the PheE11 in ligand-binding, structural stabilization and ligand migration.

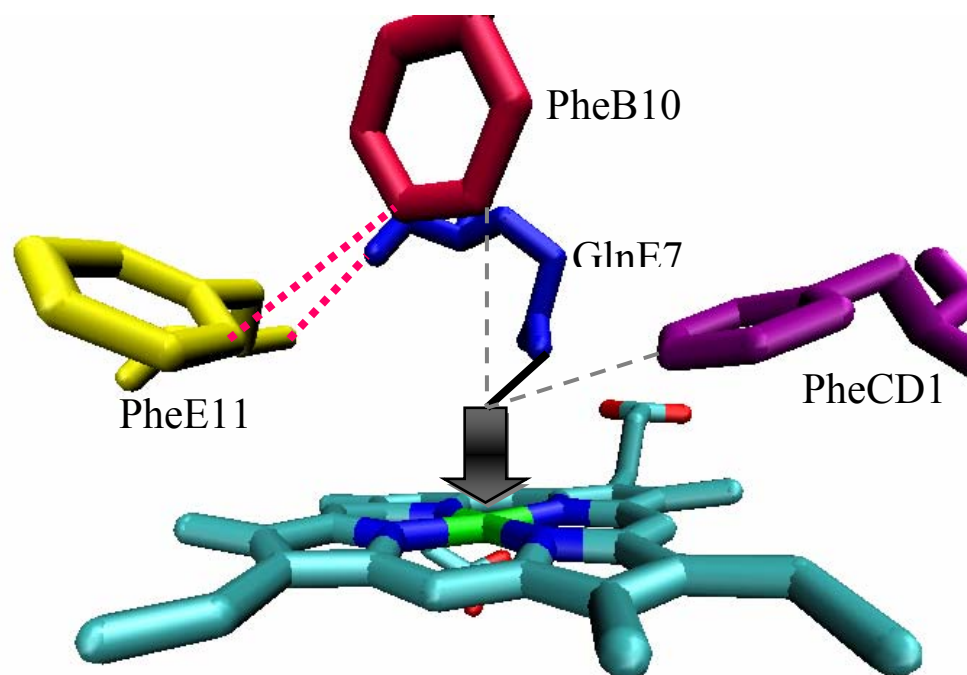


**Figure 4.3 Schematic illustration of the interactions in wt-Hbl, where the Phe at the E11, B10 and CD1 are showed in yellow, red and purple, respectively. The Gln at the E7 position is showed in blue, and the arrow represents the CO bound to the Fe. The dotted magenta lines represent the possible steric and hydrophobic interactions of the PheE11 with the GlnE7 and PheB10. The dash gray lines represent the electrostatic interactions of the Phe B10 and CD1 once the PheE11 positionated them in the right way. While the solid black line represent the possible hydrogen bond of the GlnE7 with the CO. The drawings were made with VDM 1.8.5**

## 5 CONCLUSIONS AND FUTURE WORKS

### 5.1 Conclusion

The experimental data along with site-directed mutagenesis allows us to elucidate the role of the E11 position in HbI from *Lucina pectinata*. Several stretching vibrational frequencies for the HbI PheE11Val, HbI PheE11Gln, and HbI PheE11Tyr have observed. Each of these frequencies was assigned to a different conformation; dictated by electrostatic interactions between the distal residues and bound CO. The results indicate that the mutations at the E11 position caused a structural displacement of the amino acids (B10 and E7) in the heme distal site. This structural change may allow the distal glutamine and the phenylalanine, at the E7 and B10 position respectively, to move closer to the heme binding site, making the stabilization of CO by hydrogen bonding and/or multipole interactions possible. The interactions of these residues might be induced by the movement of the E-helix, which has been observed in other hemoglobins. This is sustained with the trend observed in the association rate constants of CO and O<sub>2</sub>, along with the dissociation constant of O<sub>2</sub>. Thus, these findings strongly suggest that: (i) the PheE11 is a possible structural “controller” (maintaining distal heme volume) and (ii) its side chain is important to establish the ligand movement pathway within HbI. Therefore, the PheE11 may play a significant role in the stabilization of the H<sub>2</sub>S in HbI because allows the GlnE7 to have hydrogen bonding with the H<sub>2</sub>S.

## 5.2 Future Works

For a better understanding of the ligand-binding, structure-function relationship of HbI, could be studied, such as: (i) Kinetic studies at different CO and NO concentration - to verify the mechanism of the CO dissociation in HbI (ii) Resonance Raman - to validate the existence of the residue-ligand and residue-residue interactions. (iii) FT-IR with double and triple HbI mutants - to verify the role of the residues including the CD1, (iv) X-Ray diffraction of HbI-CO and HbI-O<sub>2</sub> complexes, and (v) Molecular dynamic simulations with CO bound to the heme iron.

## REFERENCES

1. Weber, R.E., and Vinogradov, S.N. (2001) Nonvertebrate hemoglobins: function and molecular adaptations, *Physiological Reviews* 81, 570-616.
2. Egawa, T., and Yeh, S. (2005) Structural and functional properties of hemoglobins from unicellular organisms as revealed by resonance Raman spectroscopy, *J. Inorganic Biochemistry* 99, 72-96.
3. Springer, B.A., Sligar, S.G., Olson, J.S., and Phillips, G.N. (1994) Mechanism of ligand recognition in myoglobin, *Chem. Rev.* 94, 699-714.
4. Dougherty, D. (1996) Cation- $\pi$  Interactions in Chemistry and Biology: A New View of Benzene, Phe, Tyr, and Trp. *Science* 271, 163-168.
5. Antonini, E., and Brunori, M. Hemoglobin and myoglobin in their reactions with ligands, London and New York, 1971.
6. Kotani, M., Noda, H., Yomosa, S. and Hatano, M. (1978) Newer Approaches to Heme Proteins (Chapter I Introductory Note and Chapter II Electronic Aspects of the Heme). *Y. Adv. In Biophys.*, 11, 153-196.
7. Gouterman, M. (1959). Study of the Effects of Substitution on the Absorption Spectra of Porphin. *J Chem. Phys.* 30, 1139-1160.
8. Jung, C. (2000) Insight into protein structure and protein-ligand recognition by FTIR *J. Molec. Recognition* 13, 325-351.
9. Olchowicz, J.C., Coles, D.R., Kain, L.E., and MacDonald, G. (2002) Using infrared spectroscopy to investigate protein structure, *J. Chem. Ed.* 79, 369-371.
10. Spiro, T.G., and Wasbotten, I.H. (2005) CO as vibrational probe of heme protein active sites, *J. Inorg. Biochem.* 99, 34-44.
11. Li, T., Quillin, M.L., Phillips, G.N., and Olson, J.S. (1994) Structural determinants of the stretching frequency of CO bound to myoglobin, *Biochemistry*, 33, 1433-1446.
12. Phillips, G. N., Jr., M. L. Teodoro, T. Li, B. Smith, and J. S. Olson. (1999) Bound CO is a molecular probe of electrostatic potential in the distal pocket of myoglobin. *J. Phys. Chem. B.* 10, 8817-8829.
13. Kraus, D.W., and Wittenberg, J.B. (1990) Hemoglobins of the *Lucina pectinata*/bacteria symbiosis, *J. Biol. Chem.* 265, 16043-16053.
14. M. Kashiba, M. Kajimura, N. Goda, M. Suematsu (2002) From O<sub>2</sub> to H<sub>2</sub>S: a landscape view of gas biology, *Keio. J. Med.* 51, 1-10.
15. D. Boehning, S.H. Snyder, Novel neural modulators(2003) *Annu Rev Neurosci.* 26, 105-31.
16. Rizzi, M., Wittenberg, J.B., Coda, A., Fasano, M., Ascenzi, P., and Bolognesi, M. (1994) Structure of the sulfide-reactive hemoglobin from the clam *Lucina pectinata*, *J. Mol. Biol.* 244, 86-99.
17. Antommattei-Pérez, F.M., Rosado-Ruiz, T., Cadilla, C.L., and López-Garriga, J. (1999) The cDNA-derived amino acid sequence of hemoglobin I from *Lucina pectinata*, *J. Protein Chem.* 18, 831-836.

18. Cerda, J., Echevarría, Y., Morales, E., and López-Garriga, J. (1999) Resonance Raman studies of the heme-ligand active site of hemoglobin I from *Lucina pectinata*, *Biospectroscopy* 5, 289-301.
19. La Mar, G.N., Nguyen, B.D., Xuefeng, Z., and Krishnamurthi, V. (1998) Solution and crystal structures of a sperm whale myoglobin triple mutant that mimics the sulfide-binding hemoglobin from *Lucina pectinata*, *J. Biol. Chem.* 273, 9517-9526.
20. Silfa, E., Almeida, M., Cerda, J., Wu, S., and López Garriga, J. (1998) Orientation of the heme vinyl groups in the hydrogen sulfide-binding hemoglobin I from *Lucina pectinata*, *Biospectroscopy* 4, 311-326.
21. Cerda-Colón, J.F., Silfa, E., and López-Garriga, J. (1998) Unusual rocking freedom of the heme in the hydrogen sulfide-binding hemoglobin from *Lucina pectinata*, *J. Am. Chem. Soc.* 120, 9312-9317.
22. Navarro, A.M., Maldonado, M., González-Lagoa, J., López-Mejía, R., López-Garriga, J., and Colón, J.L. (1996) Control of carbon monoxide binding status and dynamics in hemoglobin I of *Lucina pectinata* by nearby aromatic residues, *Inorganica Chimica Acta* 243, 161-166.
23. Pietri, R., León, R.G., Kiger, L., Marden, M., Granell, L.B., Cadilla, C.L., and López-Garriga, J. (2006) Hemoglobin I from *Lucina pectinata*: A model for distal heme-ligand control, *J. Biochimica et Biophysica Acta*, 1764, 758-765.
24. G. León, H. Munier-Lehmann, O. Barzu, V. Baudin-Creuz, R. Pietri, J. López-Garriga, C.L. Cadilla (2004) High-level production of recombinant sulfide-reactive hemoglobin I from *Lucina pectinata* in *Escherichia coli*. High yields of fully functional holoprotein synthesis in the BLi5 *E. coli* strain, *Protein Expr Purif* 38, 184-95.
25. BioFlo 110 Modular Benchtop Fermentor Manual No: M1273-0054. Revision E December 16, 2002. New Brunswick Scientific Co., Inc. Pages 25-29.
26. BD TALON™ Metal Affinity Resins User Manual No: PT1320-1. Published 01 March 2004. Clontech a TAKARA BIO Company.
27. Wittenberg, J.B. (1992) Functions of cytoplasmic hemoglobins and myohemerythrin, *Adv. Comp. Environ. Physiol.* 13, 59– 85.
28. Kundu, S., Blouin, G.C., Premer, S.A., Sarath, G., Olson, J.S., and Hargrove, M.S. (2004) Tyrosine B10 inhibits stabilization of bound carbon monoxide and oxygen in soybean leghemoglobin, *Biochemistry* 43, 6241-6252.
29. Paper on preparation 2007.
30. Owrutsky, J.C., Li, M., Locke, B., and Hochstrasser, R.M. (1995) Vibrational relaxation of the CO stretch vibration in Hemoglobin-CO, Myoglobin-CO and Protoheme-CO. *J. Phys. Chem.* 99, 4842-4846.
31. Zhao, X., Vyas, K., Nguyen, B.D., Rajarathnam, K., La Mar, G.N., Li, T., Phillips, G.N., Eich, R.F., Olson, J.S., Ling, J., and Bocian, D.F. (1995) A double mutant of sperm whale myoglobin mimics the structure and function of elephant myoglobin *J. Biol. Chem.* 270, 20763-20774.

32. Rohlfs, R.J., Mathews, A.J., Carver, T.E., Olson, J.S., Springer, B.A., Egeberg, K.D., Sligar, S.G. The effects of amino acid substitution at position E7 (residue 64) on the kinetics of ligand binding to sperm whale-myoglobin (1990) *J. Biol. Chem.* 265, 3168-3176.
33. Samuni, U., Dantsker, D., Ray, A., Wittenberg, J.B., Wittenberg, B.A., Dewilde, S., Moens, L., Oullet, Y., Guertin, M., and Friedman, J.M. (2003) Kinetic modulation in carbonmonoxy derivatives of truncated hemoglobins *J. Biol. Chem.* 278, 27241-27250.
34. Bruno, S., Faggiano, S., Spyrakis, F., Mozzarelli, A., Abbruzzetti, S., Grandi, E., Viappiani, C., Feis, A., Mackowiak, S., Smulevich, G., Cacciatori, E., and Dominici, P. (2007) The reactivity with CO of AHb1 and AHb2 from *Arabidopsis thaliana* is controlled by the sital HisE7 and internal hydrophobic cavities. *J. Am. Chem. Soc.* 129, 2880-2889.
35. Fernández-Alberti, S., Bacelo, D.E., Binning, R.C., Chergui, M., and Lopez-Garriga, J. (2006) Sulfide-Binding Hemoglobins: Effects of Mutations on Active-Site Flexibility *Biophysical J.* 91, 1698-1709.
36. Dantsker, D., Roche, C., Samuni, U., Blouin, G., Olson, J.S., and Friedman, J.M. (2005) The position 68 (E11) side chain in myoglobin regulates ligand capture, bond formation with heme iron, and internal movement into the Xenon cavities *J. Biol. Chem.* 280, 38740-38740.

## APPENDIX A

### Kinetics Data Analysis

This appendix demonstrates that the analysis estimated by the computer program is adaptable to chemical kinetics equations for first-order reactions. An example of a first-order reaction is given by the following:



where S is the monitored species,  $k$  is the rate constant and P is the reaction product. Thus, the mathematical equation for this type of reaction is given by Equation A.1

$$\frac{[S]_t}{[S]_0} = e^{-kt} \quad (\text{A.1})$$

where  $[S]_t$  is the concentration of specie S at a given time,  $[S]_0$  is the concentration of specie S at time zero,  $k$  is the rate constant and  $t$  is time. If one is to monitor a physical property (P), which is proportional to the concentration or concentrations of species, Equation A.1 becomes

$$\frac{[S]_t}{[S]_0} = \frac{P_t - P_\infty}{P_0 - P_\infty} e^{-kt} \quad (\text{A.2})$$

where  $P_t$  is the value of the physical property at a given reaction time, which in this case is an instrumental reading,  $P_0$  is the physical property at time zero,  $P_\infty$  is the value of the physical property at time infinity,  $k$  is the rate constant and  $t$  is time. Then, Equation A.2 can be rearranged as:

$$P_t = (P_0 - P_\infty)e^{-kt} + P_\infty \quad (\text{A.3})$$

Since the observed physical property is absorbance (A), Equation A.3 becomes:

$$A_t = (A_0 - A_\infty)e^{-kt} + A_\infty \quad (\text{A.4})$$

where A is a specific case, where absorbance is the monitored physical property. Since, here  $(P_0 - P_\infty)$  and  $P_\infty$  are constants. Thus,  $y = A_1 e^{(-x/t_1)} + y_0$  and Equation A.4 are mathematically equivalent as shown with respective replacements here:  $(A_0 - A_\infty) = A_1$ ,  $A_\infty = y_0$ ,  $A_t = y$ ,  $t = x$ , and  $k = (t_1)^{-1}$ .